Maternal exposure to polystyrene nanoplastics causes brain abnormalities in progeny

Bohyeon Jeong
Korea Research Institute of Bioscience and Biotechnology (KRIBB)
Young-Kyoung Ryu
Korea Research Institute of Bioscience and Biotechnology (KRIBB)
Jeong Yeob Baek
Korea Research Institute of Bioscience and Biotechnology (KRIBB)
Jahong Koo
Korea Research Institute of Bioscience and Biotechnology (KRIBB)
Subin Park
Korea Research Institute of Bioscience and Biotechnology (KRIBB)
Seungjae Zhang
Konkuk University
ChiHye Chung
Konkuk University
Rumeysa Dogan
Pohang University of Science and Technology (POSTECH)
Hyung-Seok Choi
Pohang University of Science and Technology (POSTECH)
Dahun Um
Pohang University of Science and Technology (POSTECH)
Tae-Kyung Kim
Pohang University of Science and Technology (POSTECH)
Wang Sik Lee
Korea Research Institute of Bioscience and Biotechnology (KRIBB)
Kyoung-Shim Kim
Korea Research Institute of Bioscience and Biotechnology (KRIBB)
Jinyoung Jeong
Korea Research Institute of Bioscience and Biotechnology (KRIBB)
Won-Ho Shin
Korea Institute of Toxicology
Jae-Ran Lee
Korea Research Institute of Bioscience and Biotechnology (KRIBB)
Nam-Soon Kim

Korea Research Institute of Bioscience and Biotechnology (KRIBB)

Da Yong Lee (daylee@kribb.re.kr)

Korea Research Institute of Bioscience and Biotechnology (KRIBB)

Article

Keywords: polystyrene nanoplastics, neurodevelopmental defects, maternal exposure

Posted Date: January 20th, 2021

DOI: https://doi.org/10.21203/rs.3.rs-131249/v1

Version of Record: A version of this preprint was published at Journal of Hazardous Materials on November 1st, 2021. See the published version at https://doi.org/10.1016/j.jhazmat.2021.127815.

Article

Maternal exposure to polystyrene nanoplastics causes brain abnormalities in progeny

- **Authors:** Bohyeon Jeong[1,2], Young-Kyoung Ryu[3], Jeong Yeob Baek[1], Jahong Koo[1,2], Subin Park[1], Seungjae Zhang[4], ChiHye Chung[4], Rumeysa Dogan[5], Hyung-Seok Choi[5], Dahun Um[5], Tae-Kyung Kim[5], Wang Sik Lee[6], Kyoung-Shim Kim[3], Jinyoung Jeong[6,7], Won-Ho Shin[8], Jae-Ran Lee[1], Nam-Soon Kim[1], and Da Yong Lee[1,2]*

- **Institutions:**

1. Rare Disease Research Center, Korea Research Institute of Bioscience and Biotechnology (KRIBB), 125 Gwahak-ro, Yuseong-gu, Daejeon 34141, South Korea.
2. Department of Functional Genomics, KRIBB School of Bioscience, University of Science and Technology, Daejeon, South Korea.
3. Laboratory animal Resource Center, Korea Research Institute of Bioscience and Biotechnology (KRIBB), 125 Gwahak-ro, Yuseong-gu, Daejeon 34141, South Korea.
4. Department of Biological Sciences (Neurophysiology Laboratory, C-Lab), Konkuk University, 120 Neungdong-ro, Gwangjin-gu, Seoul 05029, South Korea.
5. Department of Life Sciences, Pohang University of Science and Technology (POSTECH), Pohang, South Korea.
6. Environmental Disease Research Center, Korea Research Institute of Bioscience and Biotechnology (KRIBB), 125 Gwahak-ro, Yuseong-gu, Daejeon 34141, South Korea.
7. Department of Nanobiotechnology, KRIBB School of Biotechnology, University of Science and Technology, Daejeon, South Korea.
8. Department of Predictive Toxicology, Korea Institute of Toxicology, Daejeon 34114, South Korea.

***Address correspondence to:** Da Yong Lee, PhD, Rare Disease Research Center, Korea Research Institute of Bioscience and Biotechnology (KRIBB), 125 Gwahak-ro, Yuseong-gu, Daejeon 34141, South Korea. 82-42-860-4475 (Phone); 82-42-879-8495 (FAX); daylee@kribb.re.kr (E-mail).

Abstract

As global plastic production continues to grow, microplastics released from a massive quantity of plastic wastes have become a critical environmental concern. These microplastic particles are found in a wide range of living organisms in a diverse array of ecosystems. In this study, we investigated the biological effects of polystyrene nanoplastics (PSNPs) on development of the central nervous system using cultured neural stem cells (NSCs) and mice exposed to PSNPs during developmental stages. Our study demonstrates that maternal administration of PSNPs during gestation and lactating periods altered the functioning of NSCs, neural cell compositions, and brain histology in progeny. Similarly, our in vitro study also shows PSNP-induced molecular and functional defects in NSCs. Finally, we show that the abnormal brain development caused by exposure to high concentrations of PSNPs results in neurophysiological and cognitive deficits in a gender-specific manner. Our data demonstrate the possibility that exposure to high amounts of PSNPs may increase the risk of neurodevelopmental defects.

Main

Continuous increases in global plastic consumption have resulted in the generation of a massive amount of plastic waste that finally ends up in their release and potential accumulation in the environment as tiny invisible plastic particles. These tiny plastic particles are defined as either microplastics (< 5 mm) or nanoplastics (< 1 μm) on the basis of their diameters[1]. Besides the secondary microplastics generated from degradation of a large mass of plastic waste through the process of weathering, primary micro- and nanoplastics are often purposely manufactured for a wide range of applications[2-5]. Increasing evidence shows that when they are released into the environment, these tiny plastic particles infiltrate various living organisms, particularly in the oceans, and induces toxic effects including cytotoxicity, oxidative stress, metabolic changes, and locomotion defects[6-8]. Moreover, microplastic particles are not only detected in aqueous environments, but also in a broad range of terrestrial (0.54-67,500 mg/kg; 1.3-42,960 items/kg of soil)[9] and atmospheric (0-11,130 particles/m^2/day) ecosystems[10]. Humans are at the top of the food chain; therefore, it is possible that the amount of microplastic absorbed by humans could be higher than that absorbed by other organisms. In this regard, a recent study reported that humans can absorb considerable amounts (approximately 203-312 particles/day, 74,060-121,664 particles/year) of microplastics from the environment on a daily basis through food ingestion and other routes such as inhalation and dermal exposure (0.01-66.81 g/day)[11]. In rodents, orally administered microplastics (0.1-1 mg/day) can accumulate in various organs and finally cause metabolic disorders, oxidative stress, neurotoxicity, and reduced reproduction[12,13]. In terms of the relationship between the size of plastic particles and toxicity, smaller particles have higher toxicity[14,15], although the majority of nanoplastics in the environment remain difficult to detect because of technical barriers[16,17].

Recently, environmental risks that may cause brain developmental disorders have become a critical concern, as the number of children with neurodevelopmental disorders continues to increase[18]. Compared with adults, infants and young children are far more vulnerable, as the brain and other organs are still developing. Moreover, in mammals, maternally-ingested toxic materials could possibly infiltrate the brain of progeny through breast milk, as the blood brain barrier (BBB) is not fully matured in neonatal developmental stages[19,20]. Regarding the effects of micro- and nano-sized plastics on CNS development, exposure to plastic particles causes locomotion defects in zebrafish and mice[21,22].

Moreover, polypropylene microplastics (5-10 μm diameters) and silica nanoparticles (35-70 nm diameter) are directly delivered from pregnant females to fetal organs such as blood capillaries, the liver, and the brain through trophoblast layers and the placenta during embryogenesis[23].

In this study, we examined whether exposure to polystyrene nanoplastic (PSNP) particles via maternal administration during embryonic and early postnatal stages affects neurodevelopment in mice. Furthermore, we also examined the effects of PSNPs on primary mouse neural stem cells (NSCs). We found that maternally-administered PSNPs delivered to progeny led to histological changes in the brain of the progeny at postnatal stages. Using primary NSCs, we demonstrated that PSNPs induced abnormal changes in the proliferation, multi-lineage differentiation potential, and gene expression pattern of NSCs. Finally, we showed that PSNP-induced abnormal brain development resulted in neurophysiological defects and cognitive deficits, especially in female mice.

Maternally-administered PSNPs are delivered to progeny through breast milk.

In this study, we sought to investigate the effect of PSNPs on brain development using yellow-green fluorescence (YG)-conjugated carboxylated PSNPs (50 nm diameter) in mice. To determine the effects of PSNPs on brain development, PSNPs were orally administered to pregnant and lactating female mice and the brain histology, neurophysiology, and behavior of the progeny were analyzed in the postnatal stages (**Fig. 1a**). As the majority of forebrain regions and maternal mammary glands start development around 8-10 days after fertilization[24], PSNPs were administered from embryonic day 8 (E8) until 2 weeks after birth (**Supplementary Fig. 1**). The effects of PSNPs were evaluated using a broad range of doses (0.5-1,000 μg/day) according to previous rodent studies (**Supplementary Table. 1**). Scanning electron microscopy (SEM) showed that the PSNPs had an appropriate diameter of approximately 50 nm and spherical shapes (**Supplementary Fig. 2a**). For oral administration and dose-dependency analysis of the effects of PSNPs on the brain, agarose jelly cubes containing various amounts of YG-PSNPs (0-1,000 μg/cm^3 cube) were prepared. Under both white light and fluorescence microscopy, the YG fluorescence intensity of the jelly cubes increased in association with the amount of YG-PSNPs (**Supplementary Fig. 2b**). After maternal exposure, YG signals were detected in various brain regions (sagittal view) of the postnatal progeny (P7) including the olfactory bulb, hypothalamus, with the highest intensity being detected in the hippocampus and cerebellar purkinje cell layer. However, YG signal intensity in the brainstem was far lower than in other regions. The signal intensity from the YG-PSNPs increased in a dose-dependent manner in the hippocampus and the cerebellum (**Supplementary Fig. 2c**).

To investigate the detailed absorption route and the distribution of PSNPs in the mothers and progeny at various developmental stages, we analyzed the YG signal in organs of both mothers and progeny at various time points after maternal administration of YG-PSNPs (500 μg/day). We found no YG signal in any organs of the embryos (E14) (**Fig. 1b**), or in the umbilical cord (**Fig. 1c**). Similarly, we observed very little YG signal in the fetal side of the placenta (labyrinth), whereas clear YG signals were detected in the maternal side of the placenta (decidua; **Fig. 1c**). These data suggest that maternally-administered PSNPs may not be directly absorbed by the embryo during gestation. To examine whether maternally ingested PSNPs are delivered to the progeny during neonatal and early postnatal stages, we first analyzed YG signal in the organs of lactating females and found high YG signal intensity in the

intestines, blood, and mammary glands (**Fig. 1d**). We next analyzed the organs of postnatal progeny at P1 and P7, and clearly found YG signals in the intestines, blood, and brain regions, including the hippocampus and cortex (**Fig. 1e**). Collectively, these data demonstrate that maternally-administered PSNPs were delivered to progeny through breast milk after birth, rather than being directly delivered to embryos during gestation (**Fig. 1a**).

Maternal administration of PSNPs alters the body and brain weights of offspring.

To determine the effects of PSNPs on development, we first analyzed the body and brain weights of the progeny at various developmental stages after maternal administration of PSNPs (from E8 to 2 weeks after birth; **Fig. 2a**). At 1 week after birth (P7), the body weights in the groups exposed to 100 and 500 μg of PSNPs daily were clearly higher than in the control group (**Fig. 2b and Supplementary Table. 2)**. Similarly, the groups exposed to 10, 100, and 500 μg of PSNPs daily also showed slightly higher brain weights than the control group (**Fig. 2b**). However, we did not observe an increase in either body weight or brain weight in the pups exposed to the highest dose (1,000 μg PSNPs/day). The group exposed to 1,000 μg PSNPs/day showed a decrease in body weight compared with the controls (**Fig. 2b**). This inconsistency at the highest dose could be a result of toxicity from the excessive amounts of PSNPs, even though no lethality was observed in any of the groups until 11-12 weeks after birth (data not shown). A further analysis of body weights in the postnatal individuals showed that the most significant increases in body weight occurred after administration of 100-500 μg PSNPs/day until 6 weeks after birth, with the highest increase at 6 weeks regardless of gender (**Fig. 2c and Supplementary Table. 2**). By contrast, no change was found in the weight or length of the embryos at E14 (**Fig. 2d**). Collectively, these data show that maternally-administered PSNPs abnormally altered body and brain weights of progeny in the postnatal stages.

PSNPs induce histological changes in the developing brain.

To investigate the effects of PSNPs on brain development, we performed histological analysis of the brains of the progeny at 1 w after maternal administration of PSNPs, using specific markers for various

neural cell types (**Supplementary Fig. 1**). The YG signal was clearly detectable in the hippocampus after PSNP exposure (**Fig. 3a**). As NSCs, which have self-renewal and multi-lineage differentiation potential, are the most essential cell type for brain development, we first examined whether NSCs in brain stem cell niches were altered by PSNPs. Exposure to high doses of PSNPs (500-1,000 μg/day) profoundly reduced (more than a 60% reduction) the number of Ki67+ proliferative cells in the hippocampus. In addition, progenitor cells positively labeled with nestin, a specific marker for NSCs, were also lower in the hippocampus at high doses of PSNPs (500-1,000 μg/day; **Fig. 3a**). Conversely, in the subventricular zone (SVZ) near to the lateral ventricles, we found no YG signal (**Supplementary Fig. 3a**) and no alteration in Ki67 or nestin immunostaining of NSCs after PSNP administration (**Supplementary Fig. 3b**). By genotyping of the gender with SRY primer, we confirmed that there was no gender specificity in the PSNP-induced lowering of proliferative NSCs in the hippocampus (**Supplementary Fig. 4**). These data clearly show that exposure to PSNPs alters the functioning of NSCs in the specific brain regions.

As the brain weight and proliferative NSCs in the hippocampus were clearly altered in the group treated with 500 μg/day PSNPs, we used 500 μg/day for the following analyses of neurological effects. To examine whether PSNPs alter the grey matter (which is composed of neuronal cell bodies) of the brain, we used NeuN, a marker of neuronal nuclei. We found that NeuN+ cells were lower in the hippocampal striatum radiatum and lacunosum-moleculare of PSNP-exposed mice (500 μg/day; **Fig. 3b**). Moreover, both NeuN immunolabeling and hematoxylin and eosin (H&E) staining results showed that the thickness of the neuronal layer in the hippocampal CA3 region was clearly lower in the mice exposed to PSNPs, whereas no change was observed in the CA1 and dentate gyrus of the hippocampus (**Fig. 3c**). Next, to investigate the effects of PSNPs on neuronal axons in white matter of the brain, we analyzed the histology of the corpus callosum, the largest white matter tract in the brain. Besides the neuronal soma, the thickness of the corpus callosum was also clearly lower in both the medial and lateral hemispheric regions of PSNP-exposed mice (**Fig. 3d**). Additionally, the number of GFAP+ astrocytes in white matter, including the corpus callosum and internal capsule, was remarkably higher in mice exposed to PSNPs than in control mice (**Fig. 3e**). Collectively, these data demonstrate that exposure to PSNPs during development alters not only NSC functionality, but also the number and functions of differentiated neurons and glia in the developing brain.

PSNPs cause functional abnormalities in hippocampal NSCs.

For a detailed investigation of the biological effects of PSNPs on NSC function, we chose cultured primary hippocampal NSCs as an in vitro model. As brain NSCs are proliferative multipotent stem cells, we examined the effects of PSNPs on NSC proliferation and multi-lineage differentiation ability (**Fig. 4a**) using carboxylated PSNPs (50 nm; **Fig. 4**) and large carboxylated (500 nm) PSNPs and plain PSNPs (50 and 500 nm) as well (**Supplementary Fig. 5 and 6**). We first used SEM imaging to confirm that all PSNP particles showed a suitable range of diameters (**Supplementary Fig. 5a**). Then, we examined whether the PSNP particles were evenly scattered through the culture media without aggregation. Our dynamic light scattering (DLS) analysis data clearly show that all four PSNP types had appropriate diameters without any aggregation in distilled water (DW) or the culture media used for both proliferation and differentiation until day 7 after treatment (**Supplementary Fig. 5b**). Next, we analyzed the effects of PSNPs on NSC proliferation at various doses (0-100 μg/ml) using YG-conjugated carboxylated PSNPs (50 nm diameter). We found lower total cell numbers at ≥ 10 μg/ml PSNPs (**Fig. 4b**) with no significant cell death (data not shown). On the basis of these results, we used 25 μg/ml PSNPs for the rest of our in vitro experiments because we found a clear reduction in proliferation without a cytotoxic effect at this dose.

In a detailed analysis of NSC proliferation, we found lower levels of Ki67+ proliferative cells in all four groups treated with the different types of PSNPs, with the most significant difference occurring in the group with 50 nm carboxylated PSNPs (**Fig. 4c and Supplementary Fig. 6a**). Moreover, the sizes of the neurospheres and the total numbers of cells were clearly lower in all four PSNP-exposed groups than in the controls (**Fig. 4d and Supplementary Fig. 6b**), although nestin was well expressed in all five groups (**Fig. 4c and Supplementary Fig. 6a**). To ensure that our experimental results were not limited to products from a specific company, we repeated our experiments with PSNPs (30 nm) from another company and obtained consistent results, as shown in **Supplementary Fig. 7a-d**.

Furthermore, our differentiation assay data show that the neurite length of the neurons was clearly lower in those exposed to PSNPs in vitro (**Fig. 4e and Supplementary Fig. 6c and 7e**). Similar to our in vivo data, substantially more cells differentiated into GFAP+ astrocytes following in vitro exposure to

PSNPs of all types (**Fig. 4e and Supplementary Fig. 6c and 7e**). Altogether, these data demonstrate that nanometer-sized PSNP particles lead to lower NSC proliferation and alteration of both neurogenesis and gliogenesis in the hippocampus.

The transcriptome pattern in mouse hippocampal NSCs was altered by PSNPs

To investigate the effects of PSNPs on neural development at a molecular level, we performed transcriptome analysis using mouse hippocampal NSCs exposed to 50 nm carboxylated PSNPs. Two independent replicates were analyzed for changes at the transcriptome level. Using $p < 0.05$ and 1.5-fold change (FC) filtering, we found more prominent transcriptional down-regulation than up-regulation in NSCs exposed to PSNPs (**Fig. 5a**). Gene ontology (GO) analysis showed that the majority of commonly down-regulated genes belong to the pathways related to cell division and proliferation. Many genes in this group serve as a hub, forming extensive protein-protein interactions with other proteins involved in cell cycle regulation (**Fig. 5b, c**). Of note, several kinases (e.g., *Aurka/b, Bub1,* and *Plk1*) and regulatory proteins (e.g*., Cdc20, Ccna2,* and *Ccnb1*) that are critical for cell cycle progression were identified as the major interaction hubs within the network formed by the PSNP-sensitive genes (**Fig. 5c**). This result collectively demonstrates that the PSNP-induced defects in the proliferation of NSCs and neurogenesis in the hippocampus are caused by selective down-regulation of the genes that coordinate to control cell division and proliferation.

Regarding the PSNP-induced increase in astrocytes observed in vivo and in vitro (**Fig. 3e and 4e**), we found lower mRNA expression of neurogranin (*Nrgn*) after NSCs were exposed to PSNPs (**Fig. 5d**). This observation is consistent with a previous report, which showed the number of GFAP+ astrocytes was higher in the hippocampus of *Nrgn*-deficient mice than in that of wild type mice [25]. In addition, we found increased mRNA expression of platelet-derived growth factor receptor β (*Pdgfrb*), which has implications for astrocyte reactivity and astroglioma formation[26,27], after PSNP exposure (**Fig. 5d**). Taken together, the PSNP-induced abnormal increase in astrocytes could be caused by altered expression of *Nrgn* and *Pdgfrb* genes in the developing brain.

PSNP exposure results in physiological abnormalities and cognitive deficit in a gender-dependent manner.

We next sought to examine whether PSNP-induced abnormal changes in brain structures and NSC functions were associated with functional abnormalities of the brain in adulthood by analyzing synaptic plasticity, neurotransmitters, and behavior after maternal exposure to PSNPs.

First, we investigated whether exposure to PSNP alters synaptic plasticity in the hippocampus. When long-term potentiation (LTP) was induced in the Schaffer collateral pathway of the hippocampus using theta burst stimulation (TBS), we found that LTP remained intact in both male and female mice after PSNP exposure (**Supplementary Fig. 8a**). The magnitude of the LTP did not differ between control and PSNP-exposed groups in either sex (**Supplementary Fig. 8a**; males, $p > 0.8$; females, $p > 0.9$). However, when low frequency stimulation (LFS; a well-known stimulation protocol for long term depression (LTD) induction) was given, it failed to induce any significant decrease in field excitatory postsynaptic potential (fEPSP) slopes in the PSNP-exposed groups (**Fig. 6a and Supplementary Fig. 8a**). This LTD induction failure was common to both genders when the baseline fEPSP slopes were compared with those 30 min after LFS (**Fig. 6a**). The magnitude of LTD was significantly different in PSNP-exposed female mice in comparison with controls, suggesting that the impact of PSNP exposure on bidirectional synaptic plasticity may qualitatively differ according to gender (**Fig. 6a**).

Second, to examine whether PSNPs alter neurotransmitters in the brain, we measured the amount of glutamate and GABA in the hippocampus and the cortex following exposure to PSNPs. After PSNP administration, we found 20% higher GABA in the hippocampus of female mice in comparison with controls, but did not find alteration of GABA in male mice. However, we found no change in glutamate in either the hippocampus or the cortex after PSNP administration, irrespective of gender (**Fig. 6b and Supplementary Fig. 8b**).

Third, to examine whether PSNP-induced neurophysiological alterations eventually lead to behavioral deficits, we investigated the effect of PSNPs on cognitive function using a Y-maze test and a novel object recognition test (NOT; **Fig. 6c and Supplementary Fig. 9**). The results of the Y-maze test demonstrated that only female mice exposed to PSNPs, but not male mice, had a lower alternation rate (8%) than the controls (**Fig. 6c**). Similarly, the NOT results also showed that only female progeny

exposed to PSNPs had a reduction in both exploration time (42%) and frequency (38%) in comparison with the control group (**Fig. 6c**). However, no change was found in locomotion or social interaction after PSNP administration (**Fig. 6c and Supplementary Fig. 9**). Taken together, these data suggest the possibility that exposure to high amounts of PSNPs during developmental stages may increase the risk of brain dysfunction and cognitive deficit, especially in female mice.

Conclusions

The current study demonstrates that PSNPs induce abnormalities in NSC functioning and brain development that ultimately result in neuronal dysfunction and cognitive deficit. Since the exact amount of microplastics consumed by people on a daily (or annual) basis is still unknown, we examined the effects of a wide range of doses of PSNPs according to previous studies (**Supplementary table 1**). The results demonstrated that exposure to large doses of PSNPs (≥ 500 μg/day) caused significant abnormalities in brain development, whereas low doses of PSNPs did not, suggesting that high doses of PSNPs may increase the risk of neurodevelopmental defects. In vivo and in vitro experimental approaches showed that PSNPs could increase the risk of cognitive deficit, but not that of other neurological defects such as locomotive and emotional defects. This is in contrast to previous studies showing that intake of a different type of microplastic, polyethylene microplastic, leads to anxiety and locomotion deficit in mice[22], suggesting that the action mechanisms and biological effects of microplastics may differ depending on the type of microplastic.

In this study, we found that maternally-administered PSNPs were delivered to progeny through breast milk at early postnatal stages, rather than directly to the embryos during pregnancy. This finding is consistent with previous studies showing that the placental barrier blocks polystyrene transmission to the fetus, regardless of the size or surface charge of the particles[28]. By contrast, polypropylene, silica, and titanium dioxide nanoparticles can pass through the placental barrier and directly infiltrate fetal organs[15,29]. This discrepancy could be due to differences in the properties of each nanoparticle type. Although there was no direct transmission of particles to the embryos, we commenced PSNP treatment at E8, rather than in the neonatal stages, to ensure strong accumulation of PSNPs in the mammary glands of the pregnant females, as the mammary gland undergoes development from approximately 8-9 days after fertilization[24]. In this regard, our experimental design may still include the possibility that the treatment with nanoplastics during pregnancy could have had an indirect effect on embryo development by altering the physiological state of the mother.

The female-specific cognitive impairment caused by PSNPs observed in this study may come from the sexual dimorphism of the developing brain. In this regard, gender-specific synaptic development, functioning, and neurotransmitter activity in the hippocampus have all been reported[30]. In particular, the

level of estrogen receptor α (ERα) is higher in the hippocampus of female mice than in that of male mice, and ERα signaling is a key mediator of the induction of long-term potentiation in female mice[31,32]. Consistent with these reports, we observed that PSNP exposure decreased the expression of ERα in the hippocampus of female progeny (unpublished data; data not shown). Further study is required to investigate the molecular mechanisms underlying PSNP-induced brain developmental abnormalities.

Methods

PSNPs used in the study

PSNPs used in the current study are Yellow-Green (YG)-conjugated particles with an excitation and emission wavelengths of 441 and 486 nm, respectively (Polyscience, Warrington, PA). A couple of different sizes (50 nm and 500 nm) of plain and carboxylated PSNPs (2.5% w/v aqueous suspensions) were evaluated for bioaccumulation and neurological effects. Carboxylated NPs have negatively charged carboxylate groups (COOH-) on their surfaces. Plain PSNPs have no surface modification but are negative charge stabilized colloidal particles. Aqueous suspension (2.5% w/v) of 50 nm PSNPs and 500 nm PSNPs include 3.64×10^{14} particles/ml and 3.64×10^{11} particles/ml, respectively.

Mice

Pregnant female C57BL/6J mice were purchased from Daehan Biolink Co. (Korea). Mice used in the experiment were fed AIN-93G diet to minimize autofluorescence and enhance the accuracy of tissue analysis. All animal experiments complied National Institutes of Health Guidelines and were approved by Animal Use and Care Committee protocol at Korea Research Institute Bioscience & Biotechnology (KRIBB) (Permit number: KRIBB-AEC-19193).

Treatment of PSNPs in vivo

For oral administration of PSNPs to the pregnant and lactating mother, PSNP (carboxylated; 50 nm of diameter) containing agarose jelly cubes (0-1,000 μg PSNP, 0.1 g nut powder, 10% sucrose, 2.5% agarose/cm^3 of each cube) were prepared (**Supplementary figure 2b**). PSNP containing jelly cubes were treated once a day from the 8^{th} day of pregnancy. A group of mice treated with agarose jelly cubes containing nuts and sucrose but no PSNP was used as control.

Immunofluorescence staining

Brain tissues and neurospheres were cryosectioned and immunolabeled as previously described[33,34]. Primary antibodies used in the experiments were: anti-NeuN (1:100; MilliporeSigma; Burlington, MA), anti-Neurofilament (1:500; Abcam, Cambridge, UK), anti-Ki67 (1:100; BD Biosciences, San Jose, CA), anti-Nestin (1:500; Abcam) and anti-GFAP (1:200; Thermo Fisher Scientific, Waltham, MA) antibodies. The signals were visualized with appropriate fluorescence conjugated secondary antibodies. Hoechst 33258 was used for counterstaining (Life technologies, Carlsbad, CA). The images were obtained with fluorescence microscope (Zeiss, Germany) and confocal microscope (Zeiss, Germany).

H&E staining

For histological analysis, various mouse tissues were stained with hematoxylin for nuclear staining followed by the staining with eosin to visualize cytoplasmic regions. The images were obtained using light microscope (Olympus, Japan).

Culture of mouse hippocampal NSCs

Hippocampal regions were dissected from embryonic (E16.5) mouse brain. Primary hippocampal NSCs were prepared as described previously[33,34].

Treatment of PSNPs in vitro

Biological effects of PSNPs on the functions of primary hippocampal NSCs were examined with two different sizes (50 nm and 500 nm) of carboxylated and plain PSNPs at 0-100 μg/ml. No PSNP containing distilled water was treated to the control group.

NSC proliferation assay

Neurospheres were dissociated into single cells using 0.1% Trypsin-EDTA solution. Dissociated cells

(3,000 cells/well) were seeded into 24-well ultra-low attachment plates with NSC growth medium. After 7-9 days the proliferation rate was measured as previously described[33,34].

Multi-lineage differentiation assay

Neurospheres treated with vehicle and PSNPs (25 μg/ml) were dissociated into single NSCs followed by plating onto matrigel coated-24 well culture plate (1.5 x 10^5 cells/well) with differentiation medium (DMEM/F12 media, N2, B27, Glutamax) to induce neuronal and glial differentiation. After 7-9 days, the cells were immunolabeled with anti-Tuj1 (1:1,000; Biolegend) and anti-GFAP (1:200; Thermo Fisher Scientific) antibodies for neurons and astrocytes, respectively[33,34].

Transcriptome and network analysis

For transcriptome analysis, RNA was prepared from mouse embryonic NSCs (E16.5) treated with 25 μg/ml carboxylated PSNPs (50 nm of diameter). mRNA-seq library construction was performed with MGIEasy RNA Directional Library Prep Kit (MGISEQ) according to the manufacturer's instructions. Adapter and low quality of FASTQ reads were trimmed using Trim Galore with option "-p 20". After trimming, differential gene expression analysis of mRNA-seq experiment was carried out on Tuxedo protocol[35]. Briefly, trimmed FASTQ reads were mapped to GENCODE's mm10 genome (GRCm38.p6) using Tophat[36] with options "-p 16 -r 250 -mate-std-dev 50 -library-type fr-secondstrand -G /path/ gencode.vM24.annotation.gtf". Because Tophat considers splicing junctions between exons, we used GTF file from GENCODE (gencode.vM24.annotation.gtf). To quantify gene and transcript expression, we used Cuffquant with options "-frag-bias-correct -multi-read-correct -num-threads 16 -library-type fr-secondstrand -M/path/ gencode.vM24.annotation.mask.gtf". In order to compute the gene and transcript expression more effectively, we used "-M mask file" options for ignoring all alignment within transcript in mask file. Mask file was made by linux command "grep -v 'protein coding' gencode.vM24.annotation.gtf > gencode.vM24.annotation.mask.gtf". This mask file doesn't have protein coding genes, miRNAs, and lncRNAs. We normalized the expression levels using Cuffnorm with options "-num-threads 16 -library-type fr-secondstrand -library-norm-method classic-fpkm -output-

format simple-table". To compare expression levels between control and C50nm, we used Cuffdiff with options "-frag-bias-correct -multi-read-correct -num-threads 16 -library-type fr-secondstrand -library-norm-method classic-fpkm -dispersion-method blind". We set differentially expressed gene criteria as "fold change of FPKM is more than 1.5 and p-value of Cuffdiff is less than 0.05". We called these genes differentially expressed genes (DEGs).

Gene Ontology

Gene ontology analysis was performed by Metascape with DEGs[37]. We used GO biological process, KEGG pathways, Reatome gene sets, CORUM complexes, and canonical pathways from MSigDB by default. Analysis parameters were used with enriched terms to include ≥ 3 candidates, p-value ≤ 0.01, and enrichment factor ≥ 1.5.

Protein-Protein Interaction (PPI) Network Analysis

Network analysis was performed by NetworkAnalyst[38]. We analyzed PPI based on STRING interactome database. At first, we used basic options with confidence score cutoff 900 to find out how many down-regulated DEGs are connected closely. To identify direct interaction with DEGs, we used "zero-order Network" option that shows directly connected gene.

Electrophysiology

PSNP (500 μg/day; carboxylated PSNP; 50 nm of diameter) treated mice at the age of 10-12 weeks were used for electrophysiological experiment. All animals were anesthetized by using isoflurane, and theirs brain were stored in cold choline dissection buffer (containing in mM: 110 choline chloride, 11.6 Na-ascorbate, 3.1 pyruvate, 25 $NaHCO_3$, 1.25 NaH_2PO_4, 2.5 KCl, 7 $MgCl_2$, 0.5 $CaCl_2$ and 25 glucose, bubbled with 95% O_2 and 5% CO_2). Coronal brain slices containing the hippocampus (300 mm thick) were prepared using a Leica VT1000S vibrating tissue slicer and placed in a submerged chamber with an artificial cerebrospinal fluid (aCSF, containing in mM: 1 NaH_2PO_4, 26.2 $NaHCO_3$, 118 NaCl, 2.5 KCl,

11 glucose, 2 $CaCl_2$ and 1 $MgCl_2$, bubbling with 95% O_2 and 5% CO_2) at 35°C water bath for 45 min. Brain slices were kept at room temperature before recording and transferred to the recording chamber perfusing aCSF maintained at 29-32°C. Field excitatory postsynaptic potentials (fEPSP) were recorded using a DAM-80 amplifier and WIN LTP 2.10 software (University of Bristol, UK), filtered 3 kHz and sampled at 20 kHz. Recording pipettes with resistance of 1-3MΩ were filled with aCSF. fEPSPs were obtained from CA1 dendritic areas by stimulating stratum radiatum alternatively with 20s inter-stimulation intervals by using two bipolar electric stimulators (FHC Inc, ME, USA). LTP was induced by giving 4 times of theta burst stimulation (4xTBS: a single TBS is composed of TBS, 20 bursts of 4 pulses at 100 Hz, repeated 4 times in 10s intervals). Low frequency stimulation (LFS: 600 pulses of 1Hz) was used to induce LTD[39,40].

Measurement of glutamate/GABA in the cortex and the hippocampus

For the analysis of neurotransmitters, brain tissues were isolated from 11 weeks old control and PSNP (500 μg/day; carboxylated PSNP; 50 nm of diameter) treated mice. The levels of glutamate and GABA were determined by high performance liquid chromatography (HPLC, 1260 Infinity system, Agilent Technologies, Santa Clara, CA) using an UV detector[41,42]. Briefly, the brain tissues were homogenized in distilled water and centrifuged, and the supernatants derivatized with o-phthaldialdehyde were injected using an autosampler at 4°C followed by the elution through an Eclipse Plus RR-C18 column (4.6 × 100 mm × 3.5 μm, Agilent Technologies, Santa Clara, CA) at 45±1°C with a mobile phase. The composition of the mobile phase A was 40 mM Na_2HPO_4 and 0.1% phosphoric acid, and mobile phase B was acetonitrile/methanol/water (45/45/10, v/v/v). Compounds were eluted over a 17 min runtime at a flowrate of 1 ml/min with gradient conditions (linear gradient change from 5 - 50% of mobile phase B between 0 and 15 min; 15-16 min, linear gradient change from 50 - 80% mobile phase B; 16-17 min, linear gradient change from 80% back to 5% mobile phase B). The peaks of glutamate/GABA were analyzed and integrated using a ChemStation software (Agilent Technologies, Santa Clara, CA), and all samples were normalized based on the protein concentration spectrophotometrically determined by BCA protein assay (Thermo Scientific, Waltham, MA).

Behavior tests

All the behavior tests were performed according to the time line illustrated in **supplementary figure 1**. PSNPs (500 µg/day; carboxylated PSNP; 50 nm of diameter) were maternally administered during pregnant and lactating periods (from embryonic day 8 until 2 weeks after birth) and the tests were performed in the progeny at 8-10 weeks after birth.

- *Y-maze alternation test:* The Y-maze alternation test was performed as previously described[43,44]. A Y-maze with three identical arms of plexiglass (51.5 × 11.5 × 12 cm), which were 120° apart, was used. Each mouse was placed in a Y-maze and allowed to explore the maze for 10 min. The sessions were video recorded and scored for entries into arms. The percentage of spontaneous alternation was calculated as the ratio of the actual to possible alternations (defined as the total number of arm entries minus 2), which was multiplied by 100: alternation (%) = [(number of alternation) / (total arm entries-2)] x 100.

- *Novel object recognition test (NOT):* The NOT was conducted as previously described[44]. Mice were individually habituated to a testing chamber (40 cm wide x 20 long x 20 cm high) with no objects for 5 min. Mice were placed in a testing chamber for 10 min with two identical objects (familiar objects). 24 hr later mice were placed into the testing chamber in the presence of one of the familiar objects and one novel object (novel object) for 10 min. The familiar objects were cylindrical wooden blocks 10 cm high x 2 cm diameter. The novel object was a 10 cm x 2.5 cm x 2 cm rectangular wooden block. The acquisition and recognition sessions were video-recorded and scored the time spent exploring the objects. The chambers and objects were cleaned with ethanol between trials. Exploration was defined as sniffing and touching the object with the nose and/or forepaws. Sitting on the object was not considered exploratory behaviour. A discrimination index was calculated for each animal and expressed using the following formula: (exploring the novel object - exploring the familiar object)/ (exploring the novel object + exploring the familiar object) on day 2.

- *Open field test:* The open field test was conducted as previously described[45]. Animals were habituated in the test room for 30 min before the initial testing. Mice were individually placed in an open field box (45 x 45 x 45 cm^3) for 30 min. The horizontal locomotion of the mouse was measured using a computerized video tracking system, SMART (Panlab, Barcelona, Spain).

- *Social interaction test:* Each mouse was placed in the white acryl wall box (40 x 20 x 20 cm) for 3 min for habituation. After then, an age matched novel C57BL/6J control male mouse was introduced to the test cage and allowed to explore freely for 3 min. The sessions were video recorded and social interaction, such as body sniffing, anogenital sniffing, and direct contact was analyzed for 3 min.

Statistical analysis of the data

All data were obtained from at least three replicates and analyzed by unpaired t-test or one-way ANOVA test (Newman-Keuls method). Statistical analyses were performed with GraphPad Prism (version 5.0, GraphPad Software, USA), and *p* values less than 0.05 interpreted as significant differences.

Data availability

The authors declare that the data supporting the findings of this study are available within the paper and its supplementary information files.

References

1 Shim, W. J. & Thomposon, R. C. Microplastics in the Ocean. *Arch Environ Contam Toxicol* **69**, 265-268, doi:10.1007/s00244-015-0216-x (2015).

2 Andrady, A. L. Microplastics in the marine environment. *Mar Pollut Bull* **62**, 1596-1605, doi:10.1016/j.marpolbul.2011.05.030 (2011).

3 Napper, I. E., Bakir, A., Rowland, S. J. & Thompson, R. C. Characterisation, quantity and sorptive properties of microplastics extracted from cosmetics. *Mar Pollut Bull* **99**, 178-185, doi:10.1016/j.marpolbul.2015.07.029 (2015).

4 Lehner, R., Weder, C., Petri-Fink, A. & Rothen-Rutishauser, B. Emergence of Nanoplastic in the Environment and Possible Impact on Human Health. *Environ Sci Technol* **53**, 1748-1765, doi:10.1021/acs.est.8b05512 (2019).

5 Guterres, S. S., Alves, M. P. & Pohlmann, A. R. Polymeric nanoparticles, nanospheres and nanocapsules, for cutaneous applications. *Drug Target Insights* **2**, 147-157 (2007).

6 Wesch, C., Bredimus, K., Paulus, M. & Klein, R. Towards the suitable monitoring of ingestion of microplastics by marine biota: A review. *Environ Pollut* **218**, 1200-1208, doi:10.1016/j.envpol.2016.08.076 (2016).

7 Lee, W. S. *et al.* Bioaccumulation of polystyrene nanoplastics and their effect on the toxicity of Au ions in zebrafish embryos. *Nanoscale* **11**, 3173-3185, doi:10.1039/c8nr09321k (2019).

8 Pitt, J. A. *et al.* Uptake, tissue distribution, and toxicity of polystyrene nanoparticles in developing zebrafish (Danio rerio). *Aquat Toxicol* **194**, 185-194, doi:10.1016/j.aquatox.2017.11.017 (2018).

9 Moller, J. N., Loder, M. G. J. & Laforsch, C. Finding Microplastics in Soils: A Review of Analytical Methods. *Environ Sci Technol* **54**, 2078-2090, doi:10.1021/acs.est.9b04618 (2020).

10 Zhang, Y. *et al.* Atmospheric microplastics: A review on current status and perspectives. *Earth-Science Reviews* **203**, 103118 (2020).

11 Cox, K. D. *et al.* Human Consumption of Microplastics. *Environ Sci Technol* **53**, 7068-7074, doi:10.1021/acs.est.9b01517 (2019).

12 Deng, Y., Zhang, Y., Lemos, B. & Ren, H. Tissue accumulation of microplastics in mice and biomarker responses suggest widespread health risks of exposure. *Sci Rep* **7**, 46687,

495 doi:10.1038/srep46687 (2017).
496 13 Jin, H. *et al.* Polystyrene microplastics induced male reproductive toxicity in mice. *Journal of*
497 *Hazardous Materials* **401**, 123430 (2020).
498 14 Hwang, J. *et al.* Potential toxicity of polystyrene microplastic particles. *Scientific reports* **10**, 1-
499 12 (2020).
500 15 Keelan, J. A. Nanotoxicology: nanoparticles versus the placenta. *Nature nanotechnology* **6**, 263
501 (2011).
502 16 Saliu, F. *et al.* Microplastic and charred microplastic in the Faafu Atoll, Maldives. *Marine*
503 *pollution bulletin* **136**, 464-471 (2018).
504 17 Harrison, J. P., Ojeda, J. J. & Romero-González, M. E. The applicability of reflectance micro-
505 Fourier-transform infrared spectroscopy for the detection of synthetic microplastics in marine
506 sediments. *Science of the Total Environment* **416**, 455-463 (2012).
507 18 Bennett, D. *et al.* Project TENDR: Targeting Environmental Neuro-Developmental Risks The
508 TENDR Consensus Statement. *Environ Health Perspect* **124**, A118-122, doi:10.1289/EHP358
509 (2016).
510 19 Cressman, A. M. *et al.* Maternal cocaine use during breastfeeding. *Can Fam Physician* **58**,
511 1218-1219 (2012).
512 20 Saunders, N. R., Dziegielewska, K. M., Mollgard, K. & Habgood, M. D. Physiology and
513 molecular biology of barrier mechanisms in the fetal and neonatal brain. *J Physiol* **596**, 5723-
514 5756, doi:10.1113/JP275376 (2018).
515 21 Chen, Q. *et al.* Quantitative investigation of the mechanisms of microplastics and nanoplastics
516 toward zebrafish larvae locomotor activity. *Science of the total environment* **584**, 1022-1031
517 (2017).
518 22 da Costa Araújo, A. P. & Malafaia, G. Microplastic ingestion induces behavioral disorders in
519 mice: A preliminary study on the trophic transfer effects via tadpoles and fish. *Journal of*
520 *Hazardous Materials* **401**, 123263 (2020).
521 23 Ragusa, A. *et al.* Plasticenta: Microplastics in Human Placenta. *bioRxiv* (2020).
522 24 Schwertfeger, K. L., McManaman, J. L., Palmer, C. A., Neville, M. C. & Anderson, S. M.
523 Expression of constitutively activated Akt in the mammary gland leads to excess lipid synthesis

during pregnancy and lactation. *J Lipid Res* **44**, 1100-1112, doi:10.1194/jlr.M300045-JLR200 (2003).

25 Huang, F. L. & Huang, K. P. Methylphenidate improves the behavioral and cognitive deficits of neurogranin knockout mice. *Genes Brain Behav* **11**, 794-805, doi:10.1111/j.1601-183X.2012.00825.x (2012).

26 Bethel-Brown, C., Yao, H., Hu, G. & Buch, S. Platelet-derived growth factor (PDGF)-BB-mediated induction of monocyte chemoattractant protein 1 in human astrocytes: implications for HIV-associated neuroinflammation. *J Neuroinflammation* **9**, 262, doi:10.1186/1742-2094-9-262 (2012).

27 Lafuente, J. V. *et al.* Expression of vascular endothelial growth factor (VEGF) and platelet-derived growth factor receptor-beta (PDGFR-beta) in human gliomas. *J Mol Neurosci* **13**, 177-185, doi:10.1385/JMN:13:1-2:177 (1999).

28 Grafmueller, S. *et al.* Transfer studies of polystyrene nanoparticles in the ex vivo human placenta perfusion model: key sources of artifacts. *Sci Technol Adv Mater* **16**, 044602, doi:10.1088/1468-6996/16/4/044602 (2015).

29 Yamashita, K. *et al.* Silica and titanium dioxide nanoparticles cause pregnancy complications in mice. *Nature nanotechnology* **6**, 321-328 (2011).

30 Cahill, L. Why sex matters for neuroscience. *Nat Rev Neurosci* **7**, 477-484, doi:10.1038/nrn1909 (2006).

31 Wang, W. *et al.* Memory-Related Synaptic Plasticity Is Sexually Dimorphic in Rodent Hippocampus. *J Neurosci* **38**, 7935-7951, doi:10.1523/JNEUROSCI.0801-18.2018 (2018).

32 Smith, C. C. & McMahon, L. L. Estrogen-induced increase in the magnitude of long-term potentiation occurs only when the ratio of NMDA transmission to AMPA transmission is increased. *J Neurosci* **25**, 7780-7791, doi:10.1523/JNEUROSCI.0762-05.2005 (2005).

33 Kim, T. H. *et al.* Copine1 regulates neural stem cell functions during brain development. *Biochem Biophys Res Commun* **495**, 168-173, doi:10.1016/j.bbrc.2017.10.167 (2018).

34 Jeong, B. *et al.* Spastin Contributes to Neural Development through the Regulation of Microtubule Dynamics in the Primary Cilia of Neural Stem Cells. *Neuroscience* **411**, 76-85, doi:10.1016/j.neuroscience.2019.05.024 (2019).

553 35 Trapnell, C. *et al.* Differential gene and transcript expression analysis of RNA-seq experiments
554 with TopHat and Cufflinks. *Nat Protoc* **7**, 562-578, doi:10.1038/nprot.2012.016 (2012).
555 36 Kim, D. *et al.* TopHat2: accurate alignment of transcriptomes in the presence of insertions,
556 deletions and gene fusions. *Genome Biol* **14**, R36, doi:10.1186/gb-2013-14-4-r36 (2013).
557 37 Zhou, Y. *et al.* Metascape provides a biologist-oriented resource for the analysis of systems-
558 level datasets. *Nat Commun* **10**, 1523, doi:10.1038/s41467-019-09234-6 (2019).
559 38 Zhou, G. *et al.* NetworkAnalyst 3.0: a visual analytics platform for comprehensive gene
560 expression profiling and meta-analysis. *Nucleic Acids Res* **47**, W234-W241,
561 doi:10.1093/nar/gkz240 (2019).
562 39 Park, H., Rhee, J., Lee, S. & Chung, C. Selectively Impaired Endocannabinoid-Dependent
563 Long-Term Depression in the Lateral Habenula in an Animal Model of Depression. *Cell Rep* **20**,
564 289-296, doi:10.1016/j.celrep.2017.06.049 (2017).
565 40 Rhee, J., Park, K., Kim, K. C., Shin, C. Y. & Chung, C. Impaired Hippocampal Synaptic Plasticity
566 and Enhanced Excitatory Transmission in a Novel Animal Model of Autism Spectrum Disorders
567 with Telomerase Reverse Transcriptase Overexpression. *Mol Cells* **41**, 486-494,
568 doi:10.14348/molcells.2018.0145 (2018).
569 41 Monge-Acuna, A. A. & Fornaguera-Trias, J. A high performance liquid chromatography method
570 with electrochemical detection of gamma-aminobutyric acid, glutamate and glutamine in rat
571 brain homogenates. *J Neurosci Methods* **183**, 176-181, doi:10.1016/j.jneumeth.2009.06.042
572 (2009).
573 42 de Freitas Silva, D. M., Ferraz, V. P. & Ribeiro, A. M. Improved high-performance liquid
574 chromatographic method for GABA and glutamate determination in regions of the rodent brain.
575 *J Neurosci Methods* **177**, 289-293, doi:10.1016/j.jneumeth.2008.10.011 (2009).
576 43 Belforte, J. E. *et al.* Postnatal NMDA receptor ablation in corticolimbic interneurons confers
577 schizophrenia-like phenotypes. *Nature neuroscience* **13**, 76-83, doi:10.1038/nn.2447 (2010).
578 44 Park, T. S. *et al.* Humulus japonicus inhibits the progression of Alzheimer's disease in a
579 APP/PS1 transgenic mouse model. *Int J Mol Med* **39**, 21-30, doi:10.3892/ijmm.2016.2804
580 (2017).
581 45 Go, J. *et al.* Piperlongumine decreases cognitive impairment and improves hippocampal

function in aged mice. *Int J Mol Med* **42**, 1875-1884, doi:10.3892/ijmm.2018.3782 (2018).

Acknowledgements

This study was supported by the grants in below:

- The KRIBB Initiative Research Program, grant number: KGM5222012
- The Brain Research Program of the National Research Foundation (NRF) funded by the Korean government (MSIT), grant numbers: NRF-2019M3C7A1031534 (D.Y.L.), NRF-2015M3C7A1029113 (J.-R.L.), and NRF-2019M3C7A1031742 (C.C.)
- Basic Science Research Program of the NRF funded by Korean government (Ministry of Education), grant number: NRF-2019R1I1A2A01063642 (D.Y.L.)
- The National Research Foundation of Korea (NRF) grant funded by the Korea government (MSIT), grant number: NRF-2019R1A2C2006740 (T.-K.K.), NRF- 2019R1A5A6099645 (T.-K.K.)
- The Basic Science Research Program through the National Research Foundation of Korea (NRF) funded by Korea government (MSIT), grant number: NRF-2019R1C1C1006084 (J.J.)

Author information

B.J. and D.Y.L. conceived the project, designed the experiments and wrote the paper. B.J. carried out the treatment of PSNP into mice, histological analysis and in vitro experiments. Y.-K.R. and K.-S.K performed the behavior tests of mice and analyzed the data. J.K., S.P. performed mouse tissue sampling and histological analysis. J.Y.B. and W.-H.S analyzed HPLC data and performed statistical analysis. S.Z. and C.C performed *ex vivo* electrophysiological recordings and analyzed the data. R.D., H-S.C., and T.-K.K. performed mRNA-seq experiments and D.U. and T.-K.K. analyzed the transcriptome data and protein-protein interaction network. W.S.L. and J.J. performed nanoparticle characterization. J.-R.L., N.-S.K and D.Y.L. supervised the project and all authors contributed to the discussion for carrying out the project.

Ethics declarations

The authors declare that they have no competing interests.

611

612 **Corresponding author**

613 Correspondence to Da Yong Lee

614

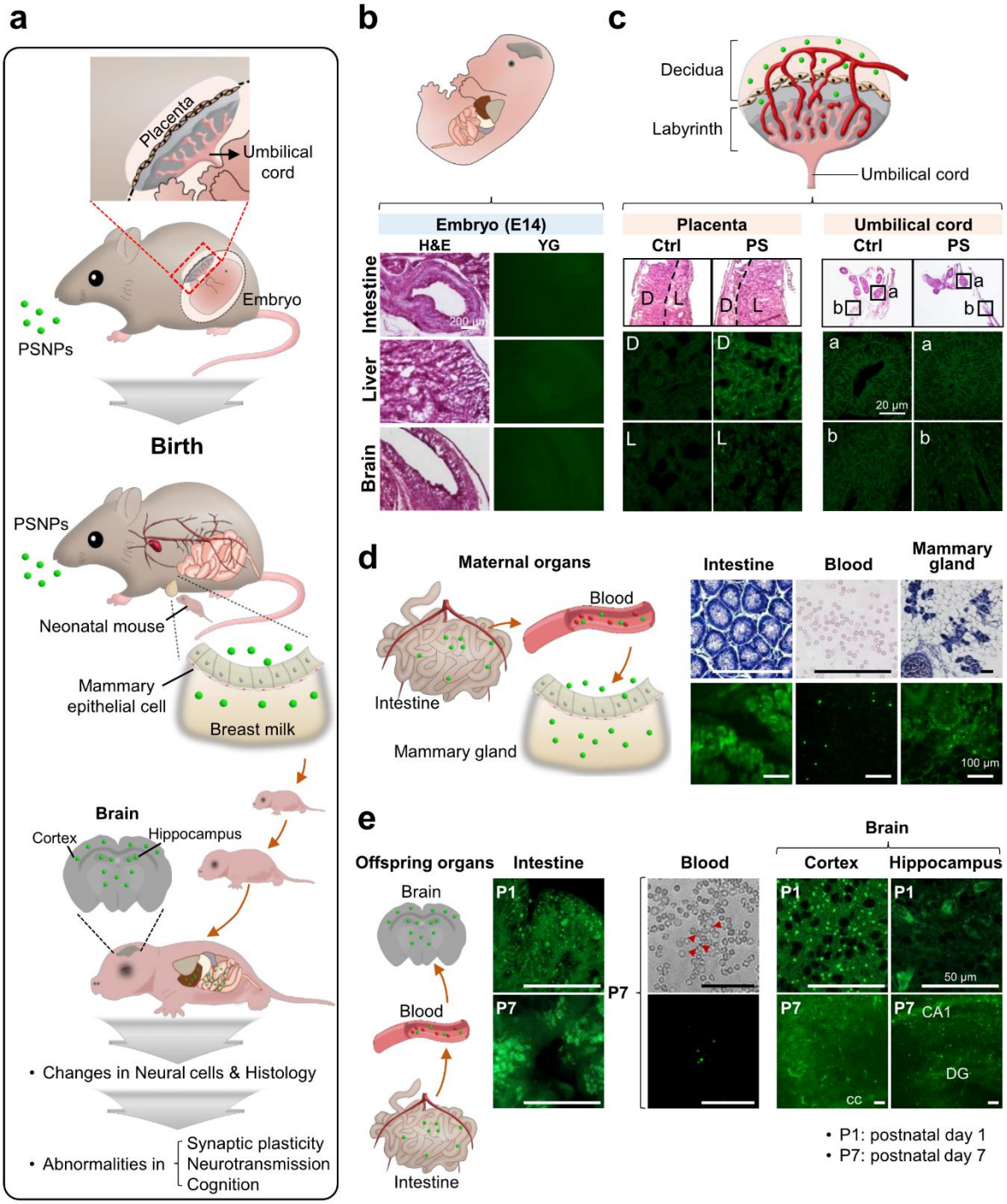
a
Placenta
Umbilical cord
Embryo
PSNPs
Birth
PSNPs
Neonatal mouse
Mammary epithelial cell
Breast milk
Brain
Cortex
Hippocampus
• Changes in Neural cells & Histology
• Abnormalities in
Synaptic plasticity
Neurotransmission
Cognition
b
Embryo (E14)
H&E
YG
Intestine
Liver
Brain
200 μm
c
Decidua
Labyrinth
Umbilical cord
Placenta
Ctrl
PS
Umbilical cord
Ctrl
PS
D
L
a
b
20 μm
d
Maternal organs
Blood
Intestine
Mammary gland
Intestine
Blood
Mammary gland
100 μm
e
Offspring organs
Intestine
Blood
Brain
Brain
Blood
Intestine
P1
P7
Cortex
Hippocampus
50 μm
CA1
DG
cc
• P1: postnatal day 1
• P7: postnatal day 7

615

616

Figure 1. Maternally-administered PSNPs infiltrated various organs of the offspring and lactating mother. (**a**) Schematic drawing shows the overall experimental procedures. (**b**) The tissue analysis data show no YG fluorescence in embryonic tissues after maternal administration of PSNPs. (**c**) YG-conjugated PSNPs were detected in the maternal side of the placenta (decidua; D), but very few were detected in the fetal side of the placenta (labyrinth; L) after PSNP administration (PS). No fluorescence signal was observed in the umbilical cord of either control group (Ctrl) or PSNP treated group (PS). Histological structures were confirmed by H&E staining. (**d**) Green fluorescence images show the accumulation of YG-conjugated PSNPs in maternal tissues including blood, intestines, and the liver. (**e**) YG-conjugated PSNPs were detected in the blood and organs of offspring at P1 and P7 including intestine, brain cortex, and hippocampus (cc: corpus callosum; DG: dentate gyrus).

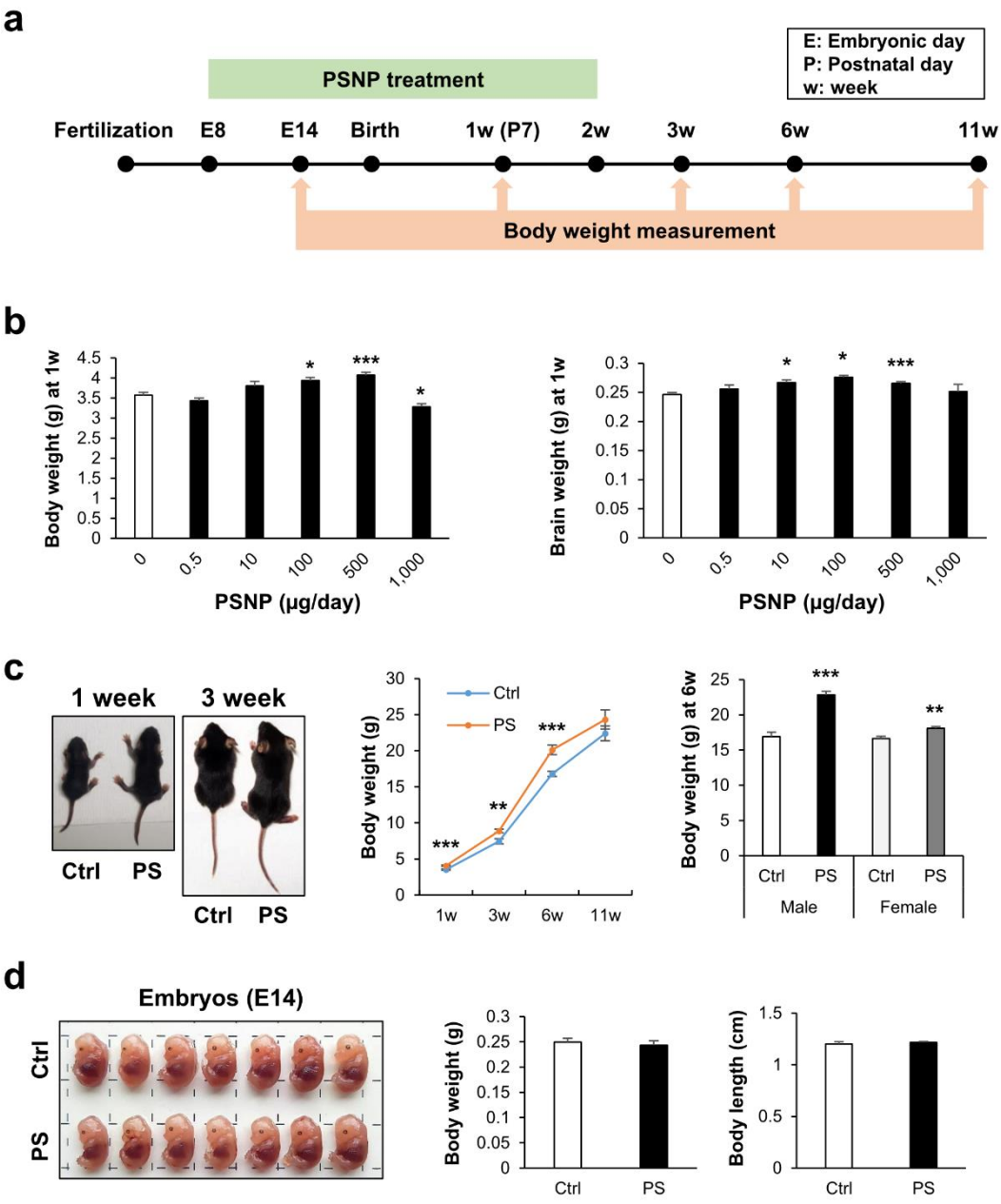
a
E: Embryonic day
P: Postnatal day
w: week
PSNP treatment
Fertilization
E8
E14
Birth
1w (P7)
2w
3w
6w
11w
Body weight measurement
b
Body weight (g) at 1w
PSNP (μg/day)
Brain weight (g) at 1w
PSNP (μg/day)
c
1 week
3 week
Ctrl
PS
Body weight (g)
Ctrl
PS
1w
3w
6w
11w
Body weight (g) at 6w
Male
Female
d
Embryos (E14)
Ctrl
PS
Body weight (g)
Body length (cm)

628

629

Figure 2. PSNPs increased the body and brain weights of the postnatal offspring. (**a**) Schematic drawing shows various time points at which body and brain weights were measured. (**b**) The PSNP-administered postnatal (1 w) group showed an increase in body weight and brain weight at doses of 100-500 μg/day. (**c**) The group that was administered 500 μg/day of PSNPs (PS) showed the highest body weight increase at 6 weeks (6 w), regardless of gender, with the difference not being any more significant at 11 weeks than in the controls (Ctrl). (**d**) No change in body weight or body length was observed in E14 embryos after PSNP treatment (PS). Values denote mean ± SEM. $*p < 0.05$, $**p < 0.005$, $***p < 0.0005$.

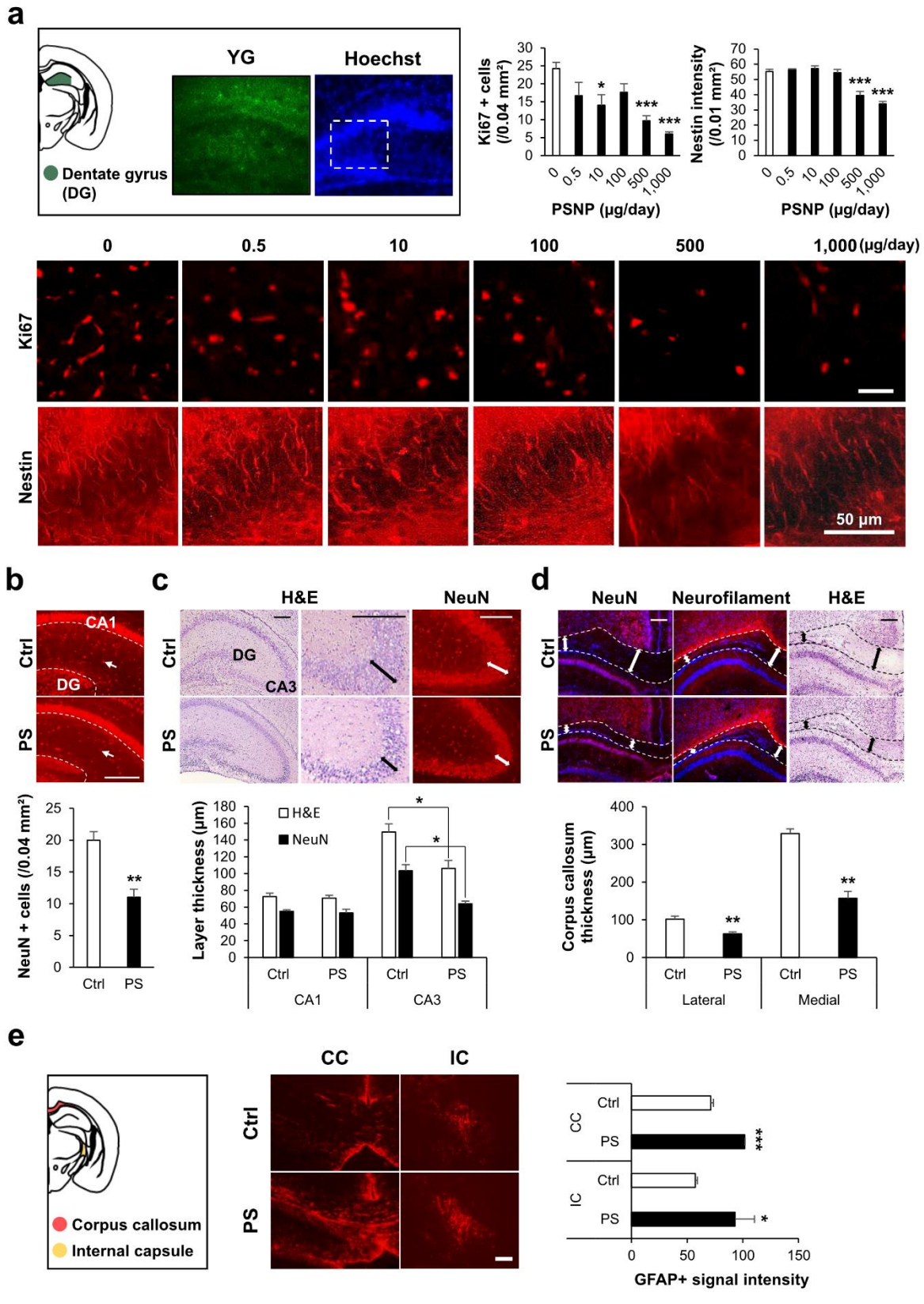
a
YG
Hoechst
Dentate gyrus (DG)
Ki67 + cells (/0.04 mm²)
Nestin intensity (/0.01 mm²)
PSNP (μg/day)
0
0.5
10
100
500
1,000 (μg/day)
Ki67
Nestin
50 μm
b
CA1
DG
Ctrl
PS
NeuN + cells (/0.04 mm²)
c
H&E
NeuN
DG
CA3
Layer thickness (μm)
H&E
NeuN
CA1
CA3
d
NeuN
Neurofilament
H&E
Corpus callosum thickness (μm)
Lateral
Medial
e
Corpus callosum
Internal capsule
CC
IC
GFAP+ signal intensity

Figure 3. PSNPs altered neural cell composition in the brains of postnatal progeny. (**a**) The mouse brain atlas shows the location of the hippocampal dentate gyrus (DG). A green fluorescence image shows the accumulation of maternally-administered YG-conjugated carboxylated PSNPs (50-nm diameter; 500 μg/day) in the hippocampus of the progeny at P7. Immunofluorescence staining results show that the number of Ki67+ and nestin+ progenitor cells was lower in the dentate gyrus of PSNP-exposed groups (carboxylated; 50-nm diameter) at ≥ 500 μg/day. The number of Ki67+ cells and the nestin signal intensity are shown graphically. (**b**) Immunofluorescence staining data show decreased NeuN+ neurons in the stratum radiatum and stratum lacunosum-moleculare of the hippocampus (*arrow*) following PSNP administration (PS). (**c**) H&E staining and NeuN immunolabeling data show reduced thickness of the hippocampal CA3 layer following 500 μg/day PSNP exposure. (**d**) Immunolabeling and H&E staining data show that the thickness of NeuN- and neurofilament+ corpus callosum was lower in mice exposed to 500 μg/day PSNP treatment. (**e**) The mouse brain atlas shows the structure of the white matter including the corpus callosum (CC) and the internal capsule (IC). Immunofluorescence staining data show that the GFAP+ signal intensity in the white matter (CC and IC) was higher in mice exposed to 500 μg/day of PSNPs. Values denote mean ± SEM. *$p < 0.05$, **$p < 0.005$, ***$p < 0.0005$. Scale bars: (**b, c**) 200 μm, (**d, e**) 100 μm.

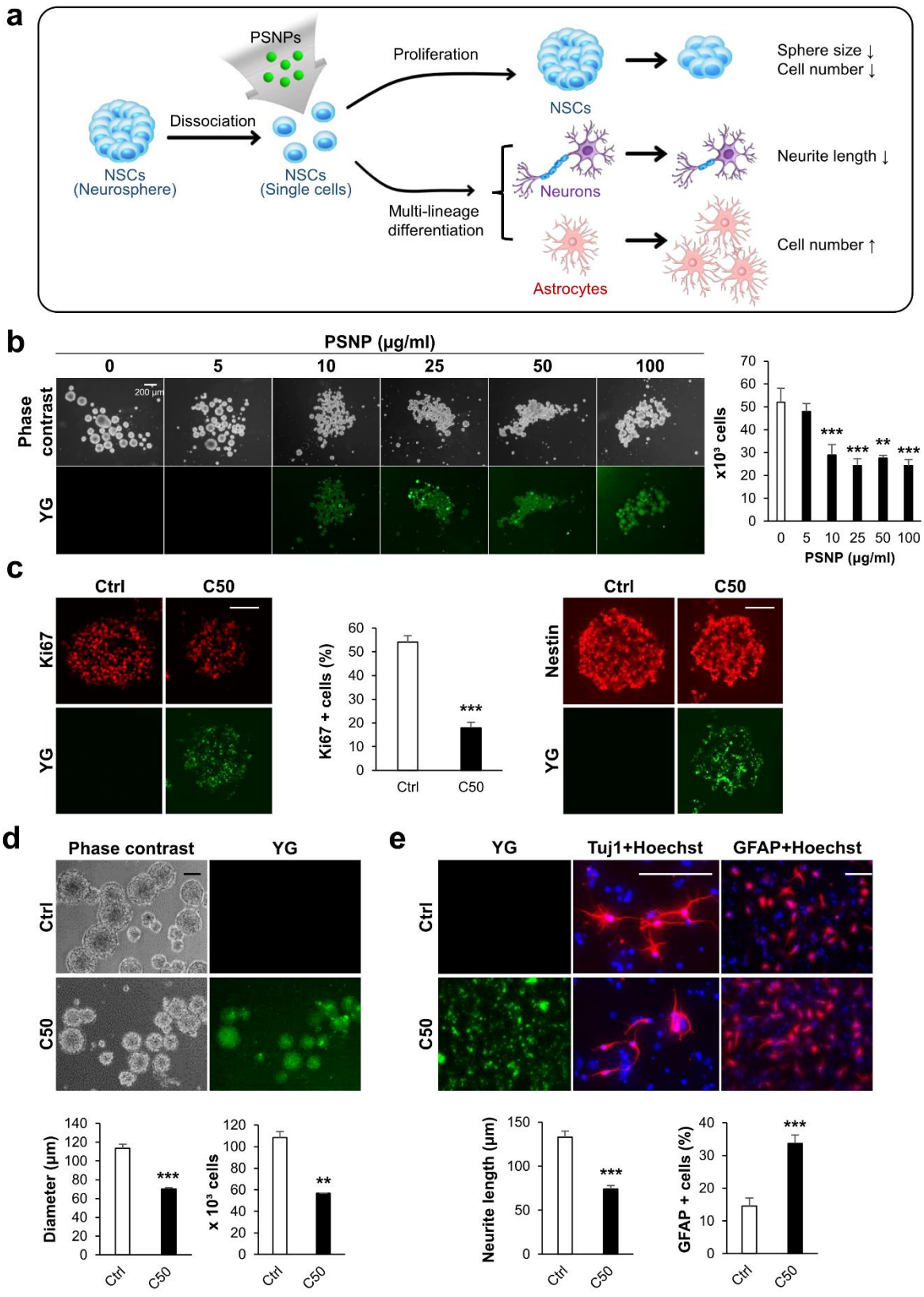
a
PSNPs
Proliferation
Dissociation
NSCs
NSCs
(Neurosphere)
NSCs
(Single cells)
Sphere size ↓
Cell number ↓
Neurons
Neurite length ↓
Multi-lineage
differentiation
Astrocytes
Cell number ↑
b
PSNP (μg/ml)
0
5
10
25
50
100
Phase contrast
YG
200 μm
x10³ cells
PSNP (μg/ml)
c
Ctrl
C50
Ki67
YG
Ki67 + cells (%)
Nestin
d
Phase contrast
YG
Diameter (μm)
x 10³ cells
e
YG
Tuj1+Hoechst
GFAP+Hoechst
Neurite length (μm)
GFAP + cells (%)

Figure 4. PSNP exposure led to impaired proliferation and multi-lineage differentiation of NSCs in vitro. (**a**) An illustration summarizing the in vitro procedure used to examine the effects of PSNPs on NSC proliferation and multi-lineage differentiation. (**b**) The total cell number of NSCs was lower after exposure to 50 nm carboxylated PSNPs at ≥ 10 μg/ml. (**c**) Immunofluorescence staining of single neurospheres shows a decrease in Ki67+ proliferative NSCs following exposure to PSNPs (C50; 25 μg/ml carboxylated PSNPs of 50 nm diameter). Other staining data show that nestin was well expressed in the neurospheres of the control (Ctrl) and PSNP-exposed groups (C50). YG fluorescence signals (green) were detected only in the PSNP-exposed group (C50). (**d**) Smaller neurosphere diameters and total cell numbers were observed in the PSNP-exposed group than in the controls (Ctrl). (**e**) NSC differentiation assay data show a decreased neurite length of Tuj1+ neurons and a significant increase in GFAP+ astrocytes in the 25 μg/ml PSNP-treated group compared with controls. C: carboxylated PSNP; 50: 50 nm. Values denote mean ± SEM. $^{**}p < 0.005$, $^{***}p < 0.0005$. Scale bars: 100 μm.

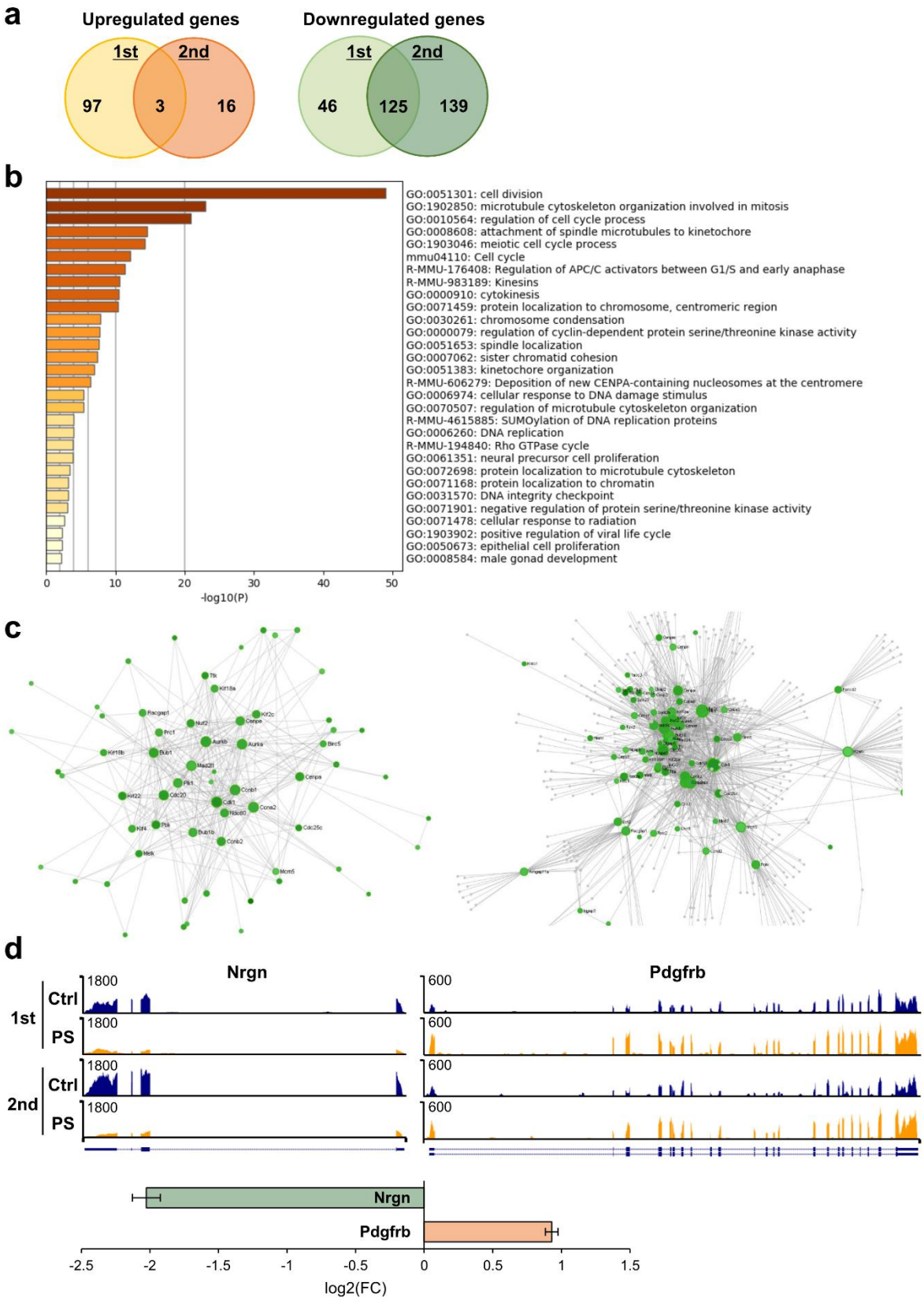
a
Upregulated genes
1st
2nd
97
3
16
Downregulated genes
1st
2nd
46
125
139
b
GO:0051301: cell division
GO:1902850: microtubule cytoskeleton organization involved in mitosis
GO:0010564: regulation of cell cycle process
GO:0008608: attachment of spindle microtubules to kinetochore
GO:1903046: meiotic cell cycle process
mmu04110: Cell cycle
R-MMU-176408: Regulation of APC/C activators between G1/S and early anaphase
R-MMU-983189: Kinesins
GO:0000910: cytokinesis
GO:0071459: protein localization to chromosome, centromeric region
GO:0030261: chromosome condensation
GO:0000079: regulation of cyclin-dependent protein serine/threonine kinase activity
GO:0051653: spindle localization
GO:0007062: sister chromatid cohesion
GO:0051383: kinetochore organization
R-MMU-606279: Deposition of new CENPA-containing nucleosomes at the centromere
GO:0006974: cellular response to DNA damage stimulus
GO:0070507: regulation of microtubule cytoskeleton organization
R-MMU-4615885: SUMOylation of DNA replication proteins
GO:0006260: DNA replication
R-MMU-194840: Rho GTPase cycle
GO:0061351: neural precursor cell proliferation
GO:0072698: protein localization to microtubule cytoskeleton
GO:0071168: protein localization to chromatin
GO:0031570: DNA integrity checkpoint
GO:0071901: negative regulation of protein serine/threonine kinase activity
GO:0071478: cellular response to radiation
GO:1903902: positive regulation of viral life cycle
GO:0050673: epithelial cell proliferation
GO:0008584: male gonad development
0
10
20
30
40
50
-log10(P)
c
d
Nrgn
Pdgfrb
1st
2nd
Ctrl
PS
1800
600
Nrgn
Pdgfrb
-2.5
-2
-1.5
-1
-0.5
0
0.5
1
1.5
log2(FC)

673

674

Figure 5. PSNPs altered the pattern of mRNA expression in mouse embryonic NSCs. (**a**) Differential gene expression (DEG) analysis data show the genes commonly up- and down-regulated by PSNPs (25 μg/ml carboxylated PSNPs of 50 nm diameter) in two biological replicates (analyzed by Cuffdiff, FPKM FC > 1.5 and $p < 0.05$). (**b**) Gene ontology analysis data show 125 genes (analyzed by Metascape, $p < 0.01$) down-regulated by PSNPs. (**c**) Protein-protein interaction (PPI) network analysis of 125 down-regulated genes by NetworkAnalyst with (left) or without (right) a “zero-order Network” parameter. (**d**) mRNA-seq tracks show mRNA read abundance for *Nrgn* and *Pdgfrb* (upper). Two biological replicates are shown. The average log2 (FC) values (Ctrl, PS) of the mRNAs are also shown (lower).

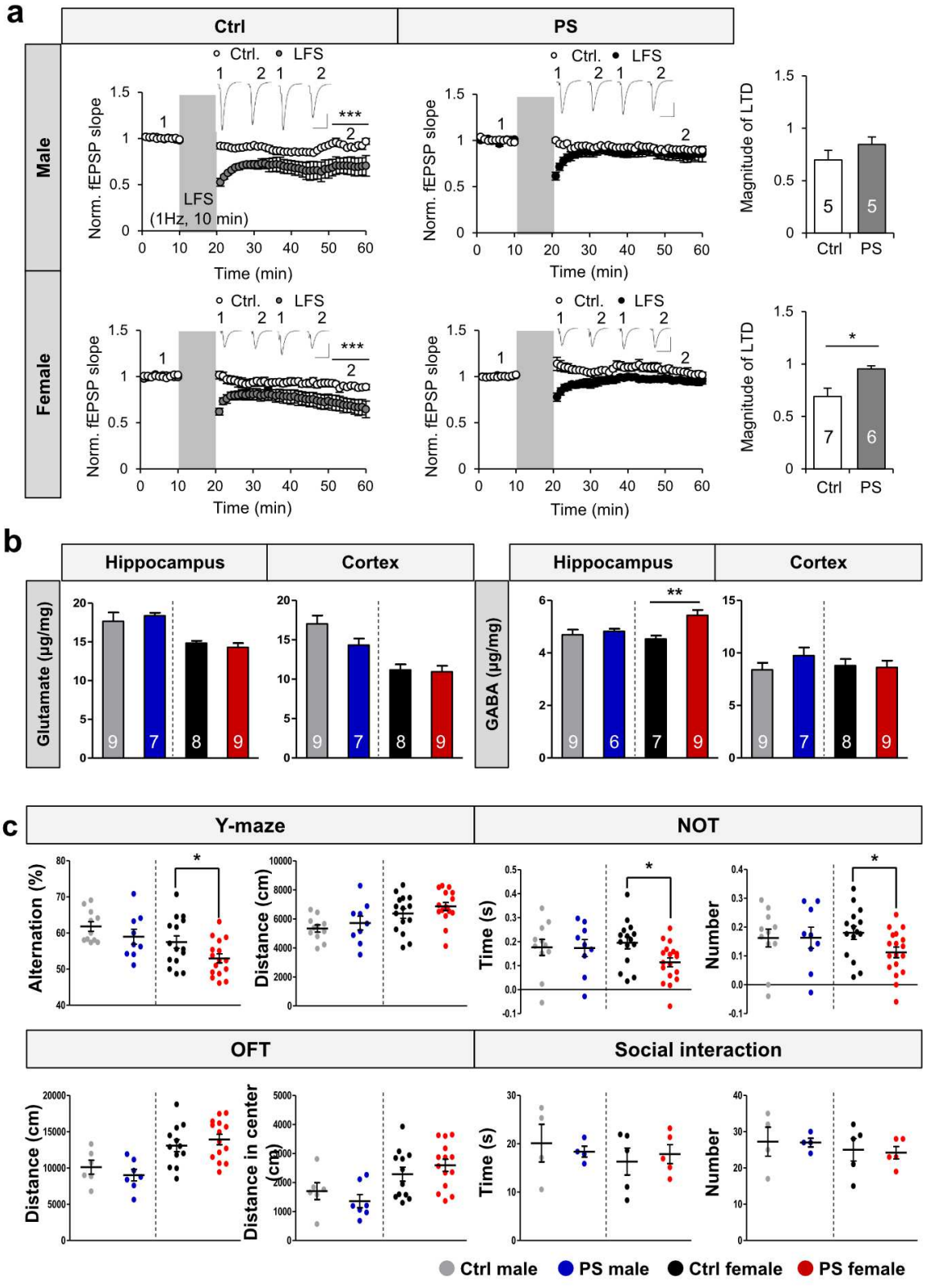
a
Ctrl
PS
Male
Female
Ctrl. LFS
Norm. fEPSP slope
LFS
(1Hz, 10 min)
Time (min)
***
Magnitude of LTD
Ctrl
PS
*
b
Hippocampus
Cortex
Glutamate (μg/mg)
GABA (μg/mg)
**
c
Y-maze
NOT
OFT
Social interaction
Alternation (%)
Distance (cm)
Time (s)
Number
Distance in center (cm)
Ctrl male
PS male
Ctrl female
PS female

685

686

Figure 6. PSNPs caused neurophysiological abnormalities and cognitive impairment in female progeny. (**a**) In comparison with baseline values, LFS decreased the rise slope of fEPSPs in control mice (8-11 weeks old; males: n = 5, 70 ± 9%, $p < 0.005$; females: n = 7, 69 ± 8%, $p < 0.01$), but not in PSNP-treated (500 µg/day) mice (8-11 weeks old; males: n = 5, 85 ± 7%, $p > 0.1$; females: n = 7, 95 ± 3%, $p > 0.1$). The average magnitude of LTD induced by LFS for the rise slope was significantly different between control and PSNP-treated (500 µg/day) female mice ($p < 0.05$). Representative traces before (1) and 35 min after (2) four episodes of TBS or LFS are shown. Scale bars: 20 ms, 0.2 mV. Values denote mean ± SEM. *$p < 0.05$, **$p < 0.01$, ***$p < 0.001$. (**b**) HPLC data show that a significant increase in the GABA level following PSNP exposure (500 µg/day) occurred only in the female hippocampus, with no change being observed in male mice. Values denote mean ± SEM. *$p < 0.05$, **$p < 0.005$. (**c**) Y-maze test results show a female-specific decrease in alternation rate in the PSNP-treated (500 µg/day) group compared with controls. NOT data show a reduction of exploration time and frequency (number) specific to the female progeny following PSNP administration. Open field test (OFT) and social interaction test results show no change in either locomotion or social activity after PSNP administration. Values denote mean ± SEM. *$p < 0.05$, **$p < 0.005$.

Figures

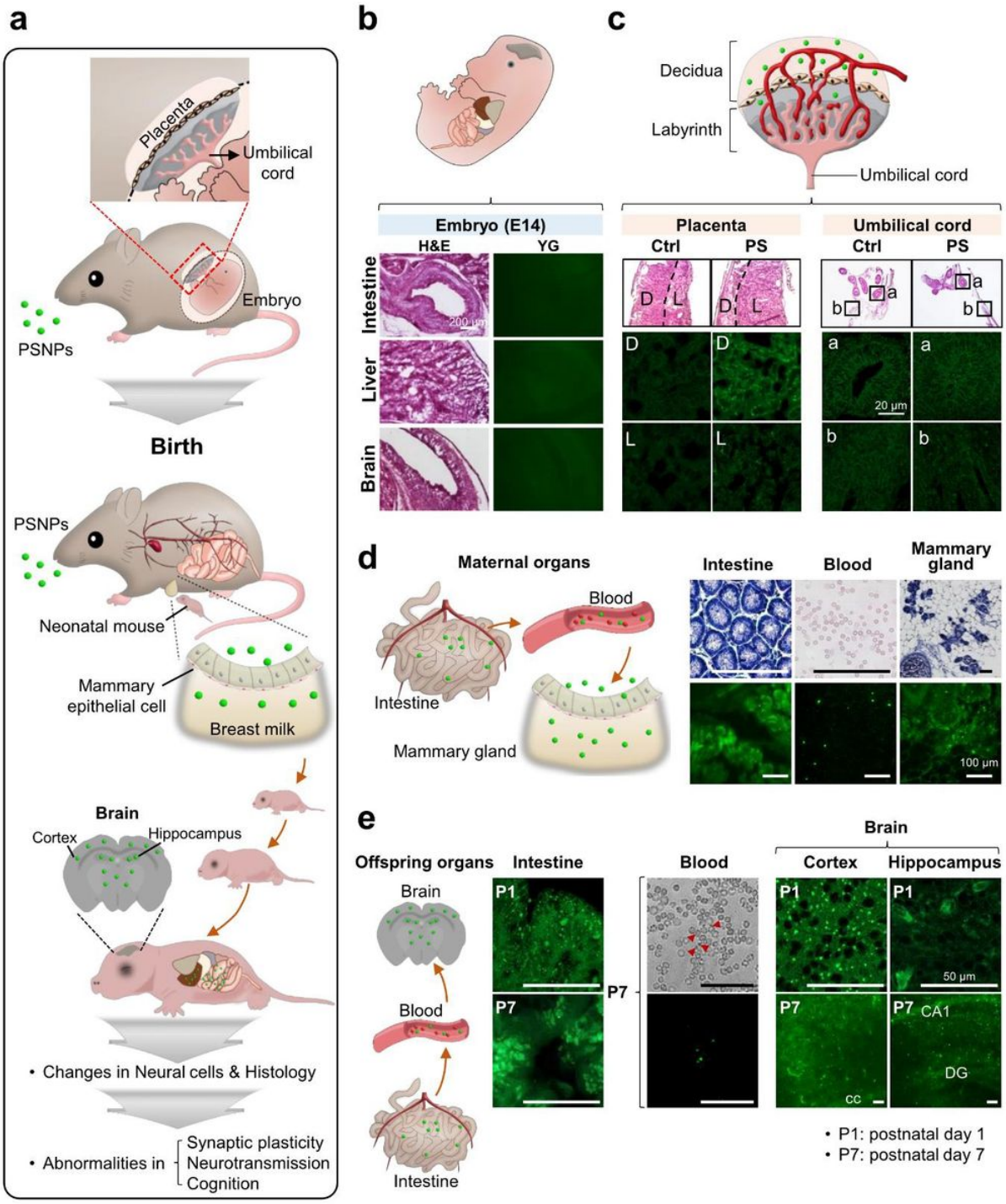

Figure 1

Maternally-administered PSNPs infiltrated various organs of the offspring and lactating mother. (a) Schematic drawing shows the overall experimental procedures. (b) The tissue analysis data show no YG fluorescence in embryonic tissues after maternal administration of PSNPs. (c) YG- conjugated PSNPs were detected in the maternal side of the placenta (decidua; D), but very few were detected in the fetal side of the placenta (labyrinth; L) after PSNP administration (PS). No fluorescence signal was observed in the umbilical cord of either control group (Ctrl) or PSNP treated group (PS). Histological structures were confirmed by H&E staining. (d) Green

fluorescence images show the accumulation of YG-conjugated PSNPs in maternal tissues including blood, intestines, and the liver. (e) YG-conjugated PSNPs were detected in the blood and organs of offspring at P1 and P7 including intestine, brain cortex, and hippocampus (cc: corpus callosum; DG: dentate gyrus).

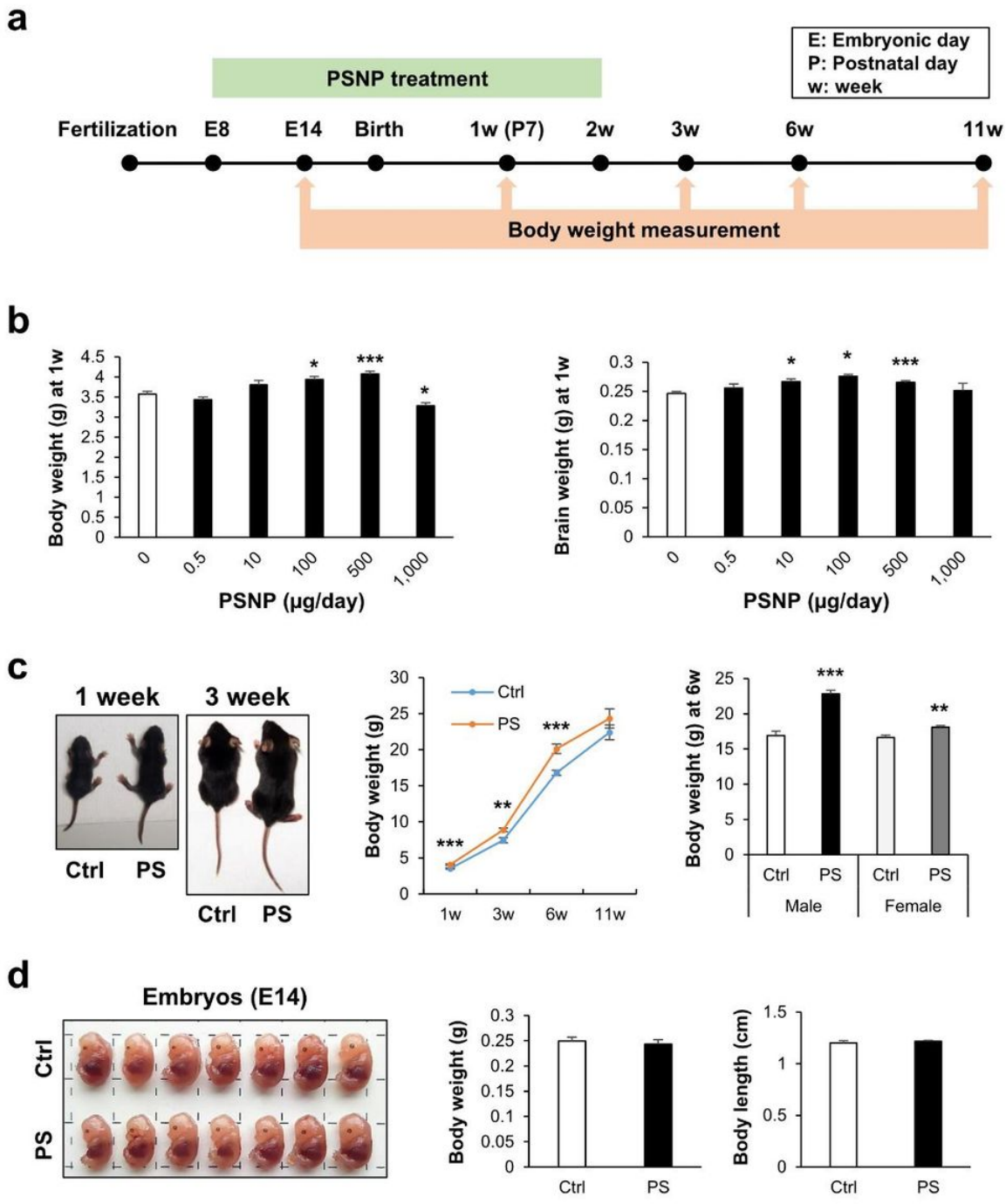

Figure 2

PSNPs increased the body and brain weights of the postnatal offspring. (a) Schematic drawing shows various time points at which body and brain weights were measured. (b) The PSNP-administered postnatal (1 w) group showed an increase in body weight and brain weight at doses of 100-500 μg/day. (c) The group that was administered 500 μg/day of PSNPs (PS) showed the highest body weight increase at 6 weeks (6 w), regardless of gender, with the difference not being any more significant at 11 weeks than in the controls (Ctrl). (d) No change in

body weight or body length was observed in E14 embryos after PSNP treatment (PS). Values denote mean ± SEM. *p < 0.05, **p < 636 0.005, ***p < 0.0005.

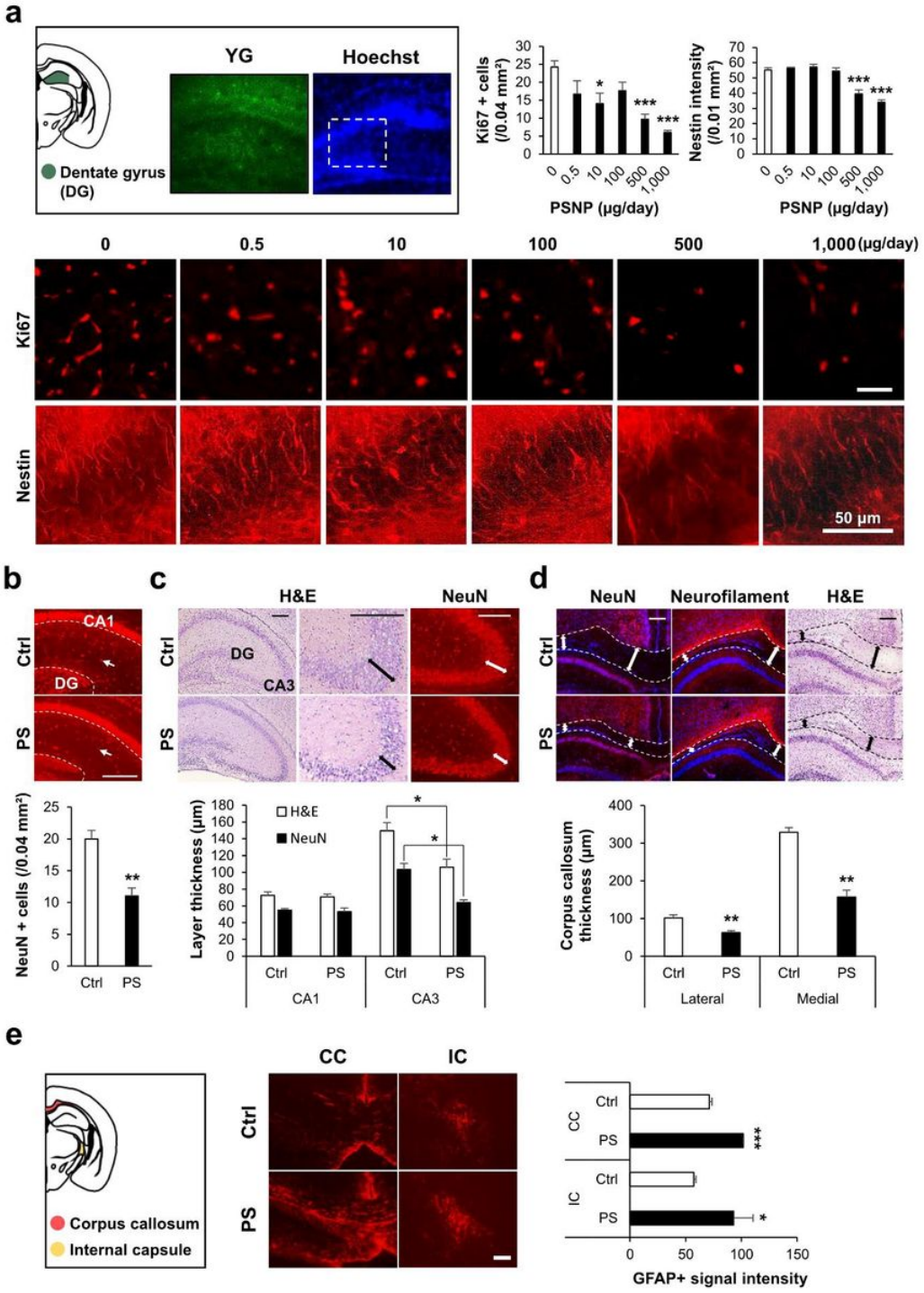

Figure 3

PSNPs altered neural cell composition in the brains of postnatal progeny. (a) The mouse brain atlas shows the location of the hippocampal dentate gyrus (DG). A green fluorescence image shows the accumulation of maternally-administered YG-conjugated carboxylated PSNPs (50-nm diameter; 500 μg/day) in the hippocampus of the progeny at P7. Immunofluorescence staining results show that the number of Ki67+ and nestin+ progenitor cells was lower in the dentate gyrus of PSNP-exposed groups (carboxylated; 50-nm diameter) at ≥ 500 μg/day. The number of Ki67+ cells and the nestin signal intensity are shown graphically. (b) Immunofluorescence staining

data show decreased NeuN+ neurons in the stratum radiatum and stratum lacunosum-moleculare of the hippocampus (arrow) following PSNP administration (PS). (c) H&E staining and NeuN immunolabeling data show reduced thickness of the hippocampal CA3 layer following 500 µg/day PSNP exposure. (d) Immunolabeling and H&E staining data show that the thickness of NeuN- and neurofilament+ corpus callosum was lower in mice exposed to 500 µg/day PSNP treatment. (e) The mouse brain atlas shows the structure of the white matter including the corpus callosum (CC) and the internal capsule (IC). Immunofluorescence staining data show that the GFAP+ signal intensity in the white matter (CC and IC) was higher in mice exposed to 500 µg/day of PSNPs. Values denote mean ± SEM. *p < 0.05, **p < 0.005, ***p < 0.0005. Scale bars: (b, c) 200 µm, (d, e) 100 µm.

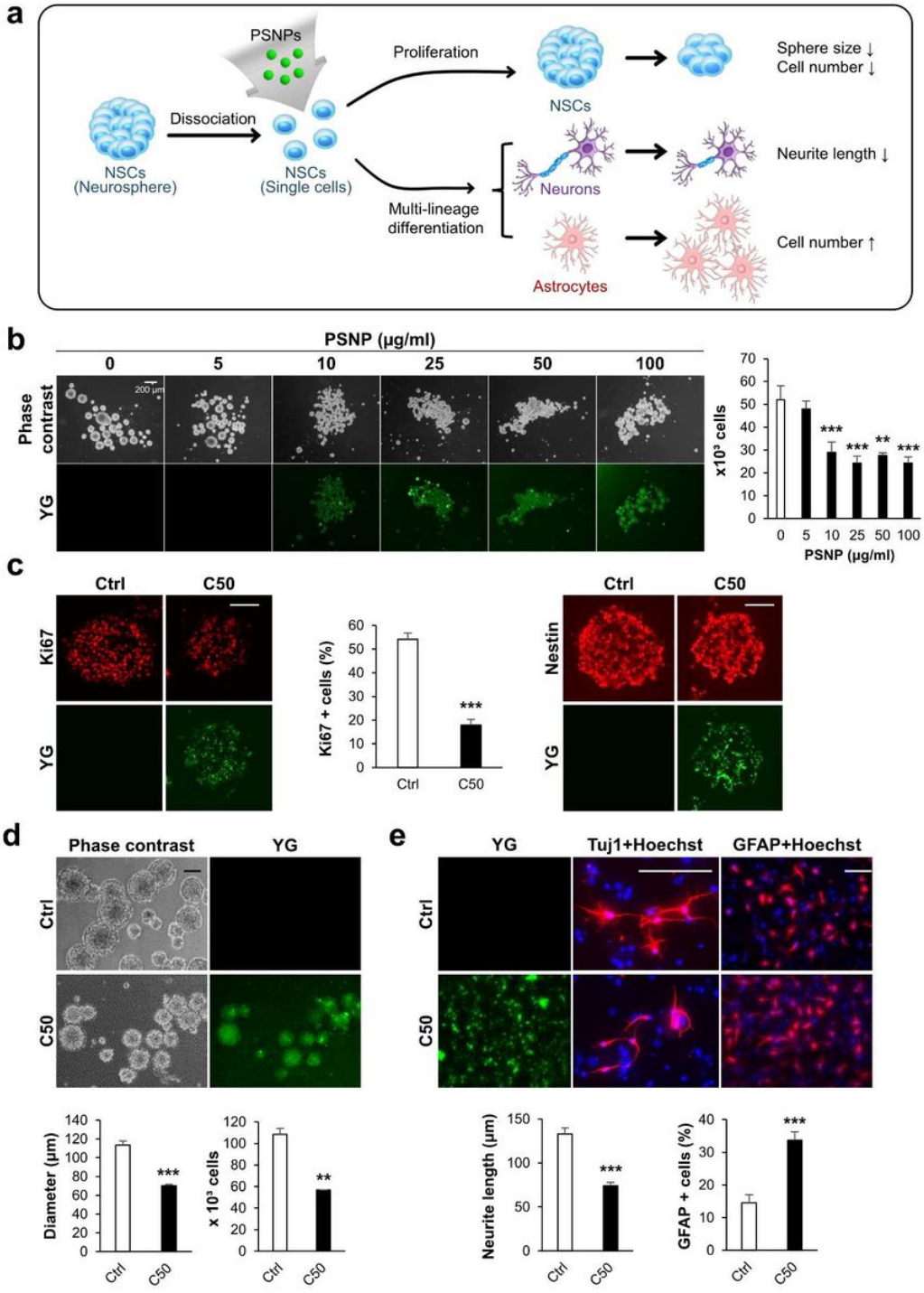

Figure 4

PSNP exposure led to impaired proliferation and multi-lineage differentiation of NSCs in vitro. (a) An illustration summarizing the in vitro procedure used to examine the effects of PSNPs on NSC proliferation and multi-lineage differentiation. (b) The total cell number of NSCs was lower after exposure to 50 nm carboxylated PSNPs at ≥ 10 μg/ml. (c) Immunofluorescence staining of single neurospheres shows a decrease in Ki67+ proliferative NSCs following exposure to PSNPs (C50; 25 μg/ml carboxylated PSNPs of 50 nm diameter). Other staining data show that nestin was well expressed in the neurospheres of the control (Ctrl) and PSNP-exposed groups (C50). YG fluorescence signals (green) were detected only in the PSNP-exposed group (C50). (d) Smaller neurosphere diameters and total cell numbers were observed in the PSNP-exposed group than in the controls (Ctrl). (e) NSC differentiation assay data show a decreased neurite length of Tuj1+ neurons and a significant increase in GFAP+ astrocytes in the 25 μg/ml PSNP-treated group compared with controls. C: carboxylated 670 PSNP; 50: 50 nm. Values denote mean ± SEM. **$p < 0.005$, ***$p < 0.0005$. Scale bars: 100 μm.

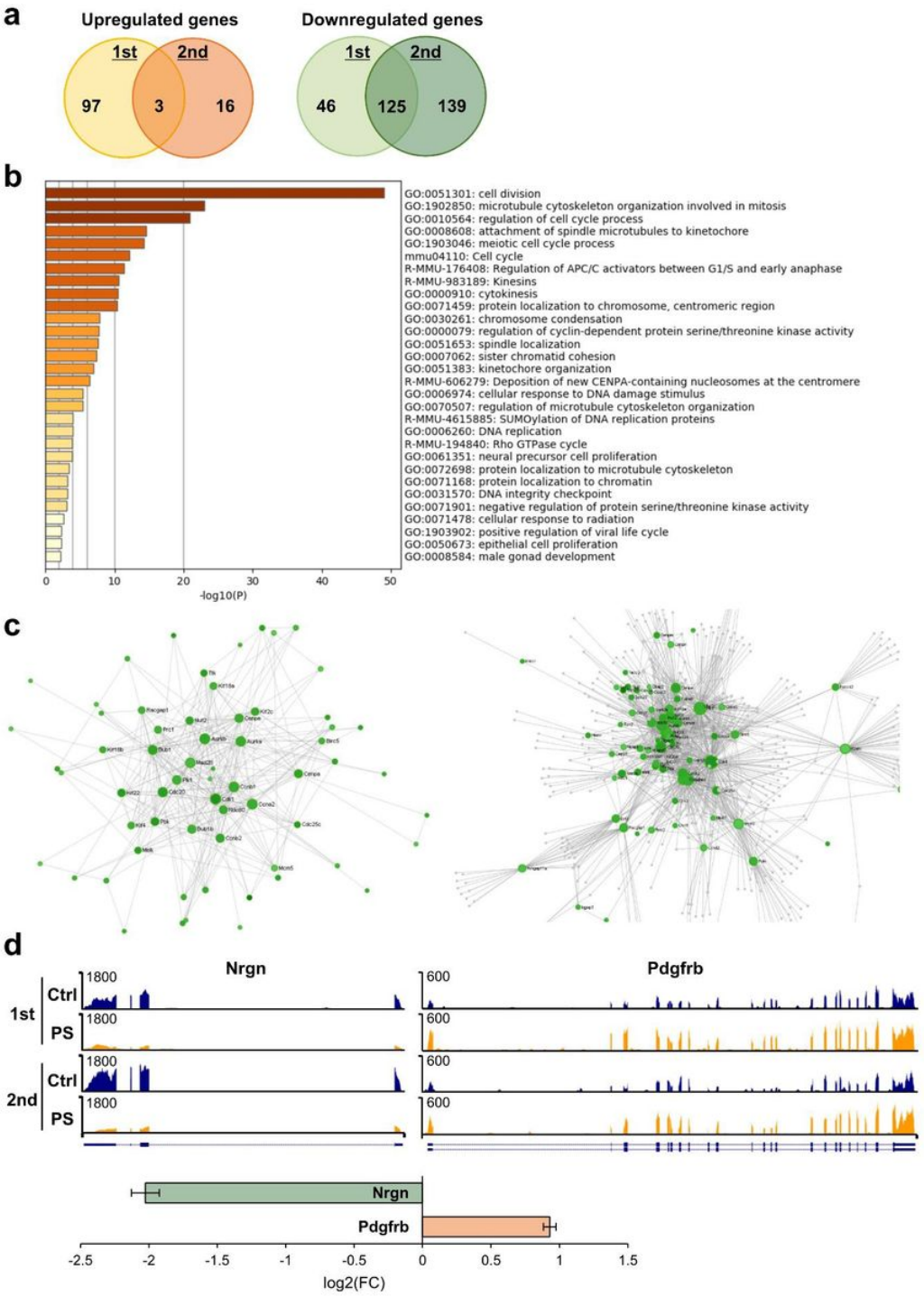

Figure 5

PSNPs altered the pattern of mRNA expression in mouse embryonic NSCs. (a) Differential gene expression (DEG) analysis data show the genes commonly up- and down-regulated by PSNPs (25 μg/ml carboxylated PSNPs of 50 nm diameter) in two biological replicates (analyzed by Cuffdiff, FPKM FC > 1.5 and $p < 0.05$). (b) Gene ontology analysis data show 125 genes (analyzed by Metascape, $p < 0.01$) down-regulated by PSNPs. (c) Protein-protein interaction (PPI) network analysis of 125 down-regulated genes by NetworkAnalyst with (left) or without (right) a “zero-order Network” parameter. (d) mRNA-seq tracks show mRNA read abundance for Nrgn and Pdgfrb (upper). Two biological replicates are shown. The average log2 (FC) values (Ctrl, PS) of the mRNAs are also shown (lower).

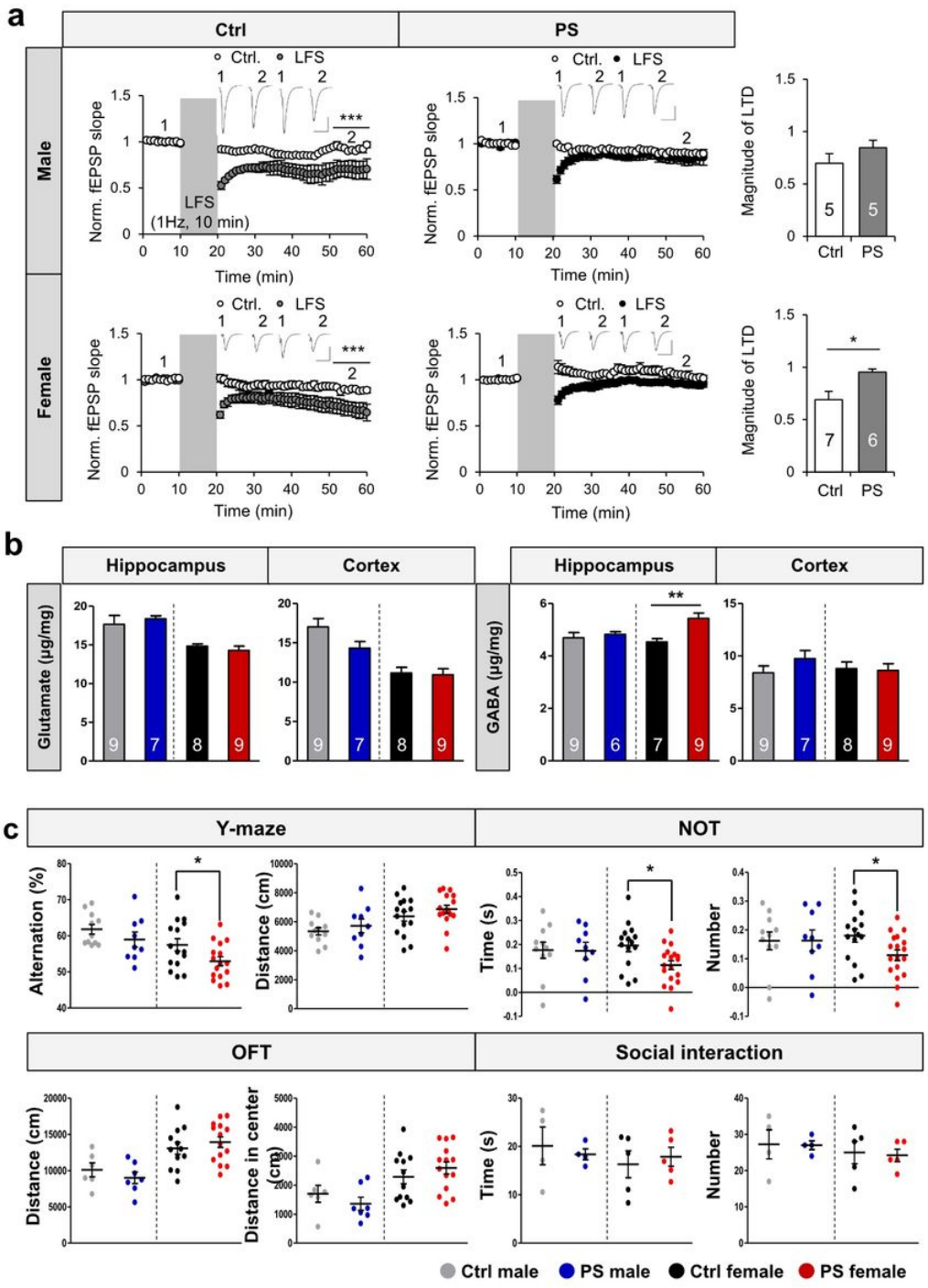

Figure 6

PSNPs caused neurophysiological abnormalities and cognitive impairment in female progeny. (a) In comparison with baseline values, LFS decreased the rise slope of fEPSPs in control (8-11 weeks old; males: n = 5, 70 ± 9%, p < 0.005; females: n = 7, 69 ± 8%, p < 0.01), but not in PSNP-treated (500 µg/day) mice (8-11 weeks old; males: n = 5, 85 ± 7%, p > 0.1; females: n = 7, 95 ± 3%, p > 0.1). The average magnitude of LTD induced by LFS for the rise slope was significantly different between control and PSNP-treated (500 µg/day) female mice (p < 0.05). Representative traces before (1) and 35 min after (2) four episodes of TBS or LFS are shown. Scale bars: 20 ms, 0.2 mV. Values denote mean ± SEM. *p < 0.05, **p < 0.01, ***p < 0.001. (b) HPLC data show that a significant increase in the GABA level following PSNP exposure (500 µg/day) occurred only in the female hippocampus, with

no change being observed in male mice. Values denote mean ± SEM. *p < 0.05, **p < 0.005. (c) Y-maze test results show a female-specific decrease in alternation rate in the PSNP-treated (500 μg/day) group compared with controls. NOT data show a reduction of exploration time and frequency (number) specific to the female progeny following PSNP administration. Open field test (OFT) and social interaction test results show no change in either locomotion or social activity after PSNP administration. Values denote mean ± SEM. *p < 0.05, **p < 0.005.

Supplementary Files

This is a list of supplementary files associated with this preprint. Click to download.

- FNaturenanotechnology2020Jeongetal1218submissionfilesSupplementaryinformationNNANO20123137.pdf